Microstructure and Microhardness Evolution in Wire Arc Additive Manufactured Al5356 All oy After High Pressure Torsion Processing

M.Tech Thesis

by

GAURAV RAJPUT

DEPARTMENT OF METALLURGICAL ENGINEERING AND MATERIALS SCIENCE (MEMS)

INDIAN INSTITUTE OF TECHNOLOGY INDORE

MAY 2025

Microstructure and Microhardness Evolution in Wire Arc Additive Manufactured Al5356 Alloy after High Pressure Torsion Processing

A THESIS

Submitted in partial fulfillment of the requirements for the award of the degree

of

Master of Technology

by

GAURAV RAJPUT

DEPARTMENT OF METALLURGICAL ENGINEERING AND MATERIALS SCIENCE (MEMS)

INDIAN INSTITUTE OF TECHNOLOGY INDORE

MAY 2025

INDIAN INSTITUTE OF TECHNOLOGY INDORE

CANDIDATE'S DECLARATION

I hereby certify that the work which is being presented in the thesis entitled **Microstructure and Microhardness Evolution in Wire Arc Additive Manufactured Al5356 Alloy after High Pressure Torsion Processing** in the partial fulfillment of the requirements for the award of the degree of **MASTER OF TECHNOLOGY** and submitted in the **DEPARTMENT OF METALLURGICAL ENGINEERING AND MATERIALS SCIENCE, Indian Institute of Technology Indore,** is an authentic record of my own work carried out during the time period from **July 2023 to May 2025** under the supervision of Dr Hemant Borkar.

The matter presented in this thesis has not been submitted by me for the award of any other degree of this or any other institute.

Gaurav Rajput 29/05/2025

Signature of the student with date
(GAURAV RAJPUT)

This is to certify that the above statement made by the candidate is correct to the best of my knowledge.

29/5/25

Signature of the Supervisor of
M.Tech. Thesis (with date)
Dr. Hemant Borkar

Gaurav Rajput has successfully given his M.Tech. Oral Examination held on **26th May 2025.**

29/5/25

Dr. Hemant Borkar
Asst. Professor, IIT Indore
Date:

29/05/2025 Acting DPGC

Convener, DPGC
Dept of MEMS
Date:

ACKNOWLEDGEMENTS

First and foremost, I would like to express my sincere gratitude to my supervisor, **Dr. Hemant Borkar**, for giving me the opportunity to work under his guidance. I am truly thankful for his constant support, encouragement, and valuable insights throughout the course of this work.

I would also like to extend my heartfelt thanks to **Dr. Ankush Marodkar** and **Dr. Hitesh Patil** for their valuable suggestions and guidance during the year. Their expertise and inputs have been instrumental in the progress of my work.

I am grateful to my **colleagues, seniors, faculty, staff, and the administration of the Department of Metallurgy Engineering and Materials Science (MEMS), IIT Indore**, for their help and cooperation throughout this journey.

Finally, I would like to thank my **family and friends** for their constant encouragement, patience, and understanding, which have always been a source of strength and motivation for me.

DEDICATION

Dedicated to my father

Abstract

Wire Arc Additive Manufacturing (WAAM) stands out for its high deposition rate and ability to produce large metal parts efficiently. Aluminum and its alloys, especially Al5356, are widely used in sectors like aerospace, automotive, construction, due to their light weight, excellent corrosion resistance, etc. However, aluminum components fabricated by WAAM often face challenges such as coarse grain structures, porosity, high residual stress, and anisotropy. These drawbacks mainly arise from the repeated thermal cycling and directional solidification during layer-by-layer deposition, which negatively impact the mechanical performance and reliability of the final product. Porosity acts as a stress concentrator that can lead to premature failure under mechanical loading, limiting the use of WAAM-fabricated parts in critical applications.

To address these limitations, this study explores the use of High-Pressure Torsion (HPT) technique as a post-processing method to enhance the structural and mechanical properties of WAAM-fabricated Al5356. HPT involves applying high pressure and torsional shear to the material, which results in ultrafine grain refinement and improved mechanical strength. The research primarily focuses on comparing the as-built WAAM samples with those treated using HPT. The microstructural features of both sets of samples will be examined using optical microscopy to observe grain structure, porosity, and interlayer bonding. The Archimedes method will be used to determine the density and surface porosity of the samples, helping assess the defects and the effectiveness of HPT in reducing them. In addition, Vickers microhardness testing will be performed to evaluate improvements in hardness due to grain refinement and strain hardening after HPT. Together, these analyses aim to provide a detailed understanding of the limitations of WAAM-fabricated Al5356 and the extent to which HPT can overcome them.

The findings of this study are expected to support the development of reliable post-processing strategies for aluminum components produced via WAAM. By demonstrating the benefits of HPT, the research contributes to the broader goal of making metal additive manufacturing more suitable for high-performance industrial applications.

Table of Contents

List of Figures

List of Tables

ACRONYMS

AM - Additive Manufacturing

WAAM - Wire Arc Additive Manufacturing

SPD - Severe Plastic Deformation

ARB - Accumulative Roll Bonding

MAF - Multi-Axial Forging

HPT - High-Pressure Torsion

ECAP - Equal Channel Angular Pressing

DED - direct energy deposition

SLM - Selective Laser Melting

EBM - Electron Beam Melting

FT – Front Transverse

SL – Side Longitudinal

Chapter 1

Introduction

The Additive Manufacturing (AM) is a material addition technique that reduces waste up to negligible levels compared to the conventional machining methods in the manufacturing industry.

After steel, aluminum is the second most used metal. The transportation, construction, food processing, and electrical industries all make extensive use of aluminum and its alloys. Its extraordinary qualities like its light weight, corrosion resistance, etc [23].

Metal additive manufacturing methods have generated attention because of their superiority over traditional manufacturing methods in creating intricate and nearly perfectly shaped components with minimal material waste. The direct energy deposition method is regarded as one of the principal techniques in metal additive manufacturing, which can be classified into powder-based and direct energy deposition [24].

The Wire Arc Additive Manufacturing (WAAM) technique might be an specialized tool for creating new materials with a particular internal structure that improves their mechanical and physical properties. The main flaw in additively produced aluminum alloys that later degrades the material's mechanical properties is porosity. The origin of cracks during fracture appears because of pores, which reduce the loading area and the material's load-carrying capacity [25]. In this regard, additional research is required to examine porosity and how it impacts the mechanical characteristics of aluminum alloys made via additive manufacturing.

One of the more extreme approaches to enhance the mechanical characteristics of WAAM materials is to apply Severe Plastic Deformation (SPD) techniques, which are known to create a distinctive microstructure and offer remarkable mechanical attributes in bulk metallic materials [26]. It has been demonstrated that ultrafine-grained structures with remarkable mechanical strength can be produced by High-Pressure Torsion (HPT) processing.

1.1 Summary and Dissertation Outline

This dissertation explores the combined use of Wire Arc Additive Manufacturing (WAAM) and High-Pressure Torsion (HPT) to enhance the microstructure and mechanical behaviour of Al5356 aluminum alloy. WAAM enables efficient layer-by-layer fabrication of large aluminum components but is often limited by internal porosity and microstructural non-uniformity. HPT, as a post-processing technique, introduces intense plastic deformation that refines the grain structure, enhances hardness, and significantly reduces porosity.

The structure of this dissertation is organized as follows. Chapter 1 introduces the fundamentals of additive manufacturing with a focus on Wire Arc Additive Manufacturing (WAAM), highlights its challenges, and presents High-Pressure Torsion (HPT) as a post-processing technique. It also describes the research motivation and objectives. Chapter 2 provides a review of the relevant literature on aluminum alloys, particularly the 5xxx series, covering both conventional and additive manufacturing methods, WAAM technology, Severe Plastic Deformation (SPD) methods, HPT processing, and porosity mitigation strategies. Chapter 3 defines the scope of the research, including the specific aims and objectives centered on evaluating the effects of HPT on WAAM-processed Al5356. Chapter 4 outlines the experimental methodology, detailing the material selection, WAAM processing, HPT post-processing, and characterization techniques such as Optical Microscopy, X-Ray Diffraction (XRD), Vickers Hardness testing, and Archimedes Density measurement. Chapter 5 presents and analyzes the experimental results, focusing on density, porosity, microhardness, XRD data, and optical microstructural evaluation. Finally, Chapter 6 summarizes the findings, discusses their implications for improving WAAM-fabricated components, and proposes directions for future research, including advanced material characterization and comparative studies using different SPD techniques.

Chapter 2

Literature Review

2.1 Potential of Al Alloys

Aluminum is the second most used metal worldwide after steel, mainly because of its beneficial characteristics such as low density, high corrosion resistance, and good thermal and electrical conductivity [1,2]. When combined with other elements to form alloys, aluminium's properties can be significantly enhanced, allowing for a wide range of mechanical performance suited for various applications. These alloys play an essential role in multiple industries including construction, transportation, marine, and aerospace. In the construction sector, they are utilized for building structures, doors, and window panels. In the automotive and aerospace fields, their lightweight nature contributes to improved fuel efficiency and reduced emissions while maintaining strength and durability. Additionally, the ability to recycle aluminum without significant loss in quality makes it an environmentally friendly option in modern engineering.

2.2 Family of Aluminum Alloy

The aluminum family is broadly classified into seven series based on their principal alloying elements and mechanical behaviour. The 1xxx series represents commercially pure aluminum with excellent corrosion resistance but relatively low strength. The 2xxx series are aluminum-copper alloys known for their high strength but reduced corrosion resistance. The 3xxx series contain manganese and offer moderate strength with good corrosion resistance. The 4xxx series, based on silicon, provide good wear resistance and moderate strength. The 5xxx series are aluminum-magnesium alloys notable for their excellent corrosion resistance and moderate to high strength. The 6xxx series, which includes aluminum-magnesium-silicon alloys, combines good strength and corrosion resistance, widely used in structural applications. Finally, the 7xxx series consists of aluminum-zinc alloys with very high strength but comparatively lower corrosion resistance [3].

Table 1.1: Family of Aluminium series [3]

Alloy Series	Major Alloying Elements	Mechanical Properties	Corrosion Resistance	Weldability	Typical Applications
1xxx	>99% Aluminum	Low strength, excellent ductility	Excellent	Excellent	Electrical conductors, chemical
2xxx	Copper	High strength, poor corrosion resistance	Poor	Poor	Aerospace, automotive
3xxx	Manganese	Moderate strength, good corrosion	Good	Good	Roofing, utensils
4xxx	Silicon	Good wear resistance, moderate strength	Moderate	Moderate	Engine components
5xxx	Magnesium	Good strength, excellent corrosion	Excellent	Excellent	Marine, automotive
6xxx	Magnesium & Silicon	Medium strength, good corrosion	Good	Excellent	Structural, architectural
7xxx	Zinc	Very high strength, poor corrosion	Poor	Poor	Aerospace, military

2.3 5xxx Al Alloys Features

Among these series, Al5356, belonging to the 5xxx series, has gained significant attention due to its balanced combination of strength, corrosion resistance, and weldability. The magnesium content in Al5356 enhances the alloy's mechanical properties and provides excellent resistance to corrosion, especially in marine and industrial environments [4]. These features make Al5356 particularly suitable for approaches to additive manufacturing, such Wire Arc Additive Manufacturing (WAAM), as well as for post-processing methods like severe plastic deformation, which can further improve its mechanical performance.

2.4 Conventional Manufacturing Methods: Casting and Rolling

Casting and rolling are traditional manufacturing methods widely used to shape aluminum alloys, including Al5356. Casting involves pouring molten aluminum into a mold in which the material solidifies to take on the required shape.. Despite its versatility and ability to produce complex geometries, casting often results in inherent defects that adversely impact the alloy's mechanical characteristics. One of the most frequent faults in cast aluminum alloys is porosity, which is mostly caused by hydrogen gas being trapped during solidification. These pores, which can be irregular or oval, function as points of stress and lower the material's overall toughness and fatigue life. [5,6]. Additionally, shrinkage cavities may form due to volumetric contraction during solidification, leading to voids in the final cast. Segregation, caused by the uneven distribution of alloying elements, produces microstructural inhomogeneity that can compromise strength and corrosion resistance. Cold shuts and misruns may also occur if the molten metal prematurely solidifies or fails to completely fill the mold cavity [5].

In Figure 2.1(a), the macroscopic cross-sectional view of the sand-cast Al–Li alloy reveals the general distribution of porosity defects across the casting. A magnified portion of this section highlights the presence of invasive pores, which exhibit irregular shapes and significant penetration into the surrounding matrix, indicating disruptions likely caused during mold filling or solidification. Image 2.1(b), corresponding to the enlarged view of area A, shows reactive pores that are presumed to form as a result of chemical interactions during solidification, such as gas generation or reactions between the molten alloy and the mold material. In contrast, Image 2.1(c), which magnifies area B, illustrates precipitation pores, typically associated with gas evolution or the formation of secondary phases during the cooling phase. These classifications and visual analyses of porosity defects are essential for understanding their underlying formation mechanisms. They provide critical insights into evaluating the integrity of the cast structure and formulating strategies for improving casting processes and minimizing defect formation in Al–Li alloys. [29]

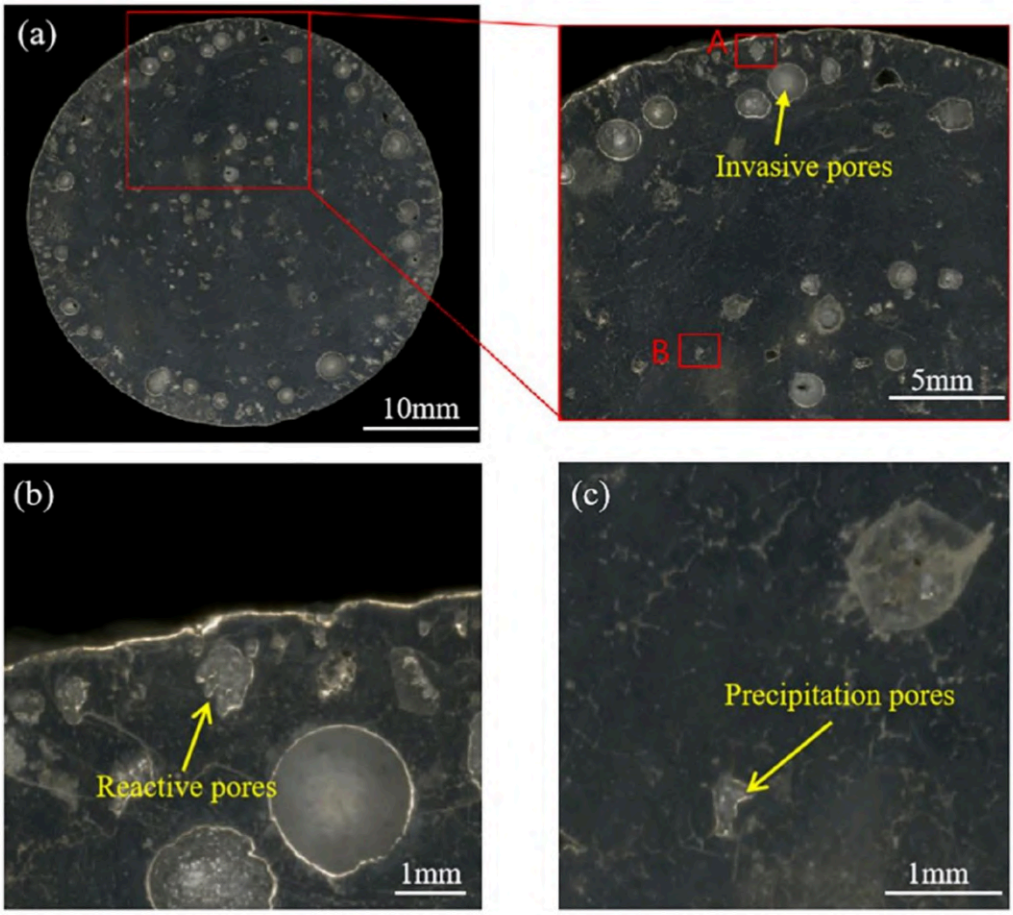

Figure 2.1 Distribution characteristics of the porosity defects of the sand casting Al–Li alloy castings: (a) Macroscopic image of area of cross-section; (b) Magnified view of area A; (c) Magnified view of area B.[29]

Rolling is a deformation process where cast ingots are compressed and passed through rollers to produce sheets or plates. This method improves the grain structure and surface finish while reducing the size and volume of some casting defects. However, rolling does not fully eliminate porosity or micro-voids; residual pores from casting may persist within the rolled product. These internal defects can limit ductility and reduce mechanical reliability under cyclic loading conditions [7,8]. Though multiple rolling passes and heat treatments can mitigate some of these issues, they often add to manufacturing time and cost. As seen in Figure 2.2, the major defects formed in sheets are shown.

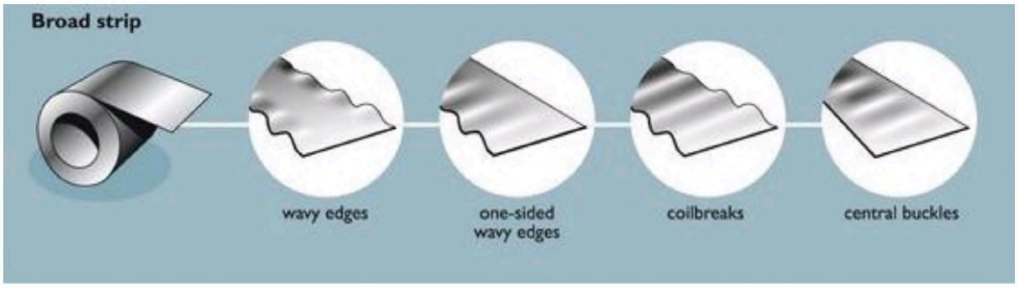

Figure 2.2 Shows the major defects that occur in rolled sheet.[27]

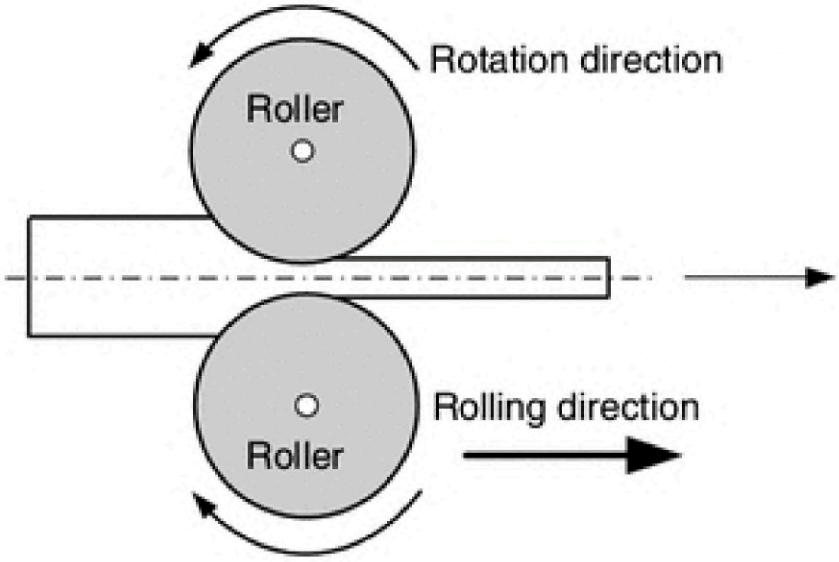

Figure 2.3: Systematic diagram for Rolling process [28]

Additive manufacturing addresses several limitations inherent to casting and rolling. By depositing material layer-by-layer and controlling the solidification locally, additive manufacturing processes reduce segregation and shrinkage defects typical in casting. The powder or wire feedstock used in additive manufacturing is melted in small, controlled volumes, allowing more uniform microstructure formation and better mechanical performance. Furthermore, the near-net-shape nature of additive manufacturing reduces the need for extensive machining and material waste [9].

2.5 Additive Manufacturing Techniques: Powder-Based and Direct Energy Deposition

Additive manufacturing (AM) encompasses several technologies that build parts layer-by-layer, primarily divided into powder-based and Direct Energy Deposition (DED) methods. Techniques like Electron Beam Melting (EBM) and Selective Laser Melting (SLM) are examples of powder-based AM. By selectively melting thin layers of aluminum powder with a laser, SLM creates dense objects with excellent mechanical qualities and exquisite microstructures [10]. EBM uses an electron beam under vacuum conditions to melt powder layers and is commonly applied in titanium but is less frequent for aluminum alloys [10]. Binder jetting is alternative powder-based method that is not as common for load-bearing aluminum parts. It entails depositing a fluid binder onto a powder bed and then sintering it.

Metal wire or powder flows directly into a melt pool produced by a concentrated energy source, like an electric arc or laser, using DED techniques. Powder-fed DED uses a nozzle to blow powder into the melt pool, allowing for detailed features but generally lower deposition rates [11]. Wire-fed DED, exemplified by Wire Arc Additive Manufacturing (WAAM), builds components layer by layer by melting aluminum wire using an electric arc. WAAM offers higher deposition rates and is well-suited for producing large components. Due to its high material efficiency, reduced powder hazards, and cost effectiveness, wire-fed DED is increasingly favored for manufacturing aluminum alloys like Al5356 [12]. To reduce frequent flaws like porosity and lack of fusion that occur in DED processes, however, exact control over processing parameters is necessary [11].

2.6 Wire Arc Additive Manufacturing (WAAM) of Al5356

In the wire-fed DED process known as WAAM, a consumable wire feedstock is melted by an electric arc, resulting in the layer-by-layer deposition of material to produce components with a near-net form. The method is cost-effective because the wire feedstock is cheaper and easier to handle compared to metal powders. WAAM's high deposition rate makes it suitable for fabricating large

and complex aluminum parts that would be challenging to produce by conventional manufacturing or other AM methods [12].

Al5356 is especially compatible with WAAM due to its good weldability and corrosion resistance conferred by magnesium. The alloy's weld pool remains stable during arc melting, reducing defects and enabling a consistent build [12]. Nevertheless, porosity remains a key challenge in WAAM parts. Gas porosity, usually spherical, occurs predominantly in the front wall of the molten pool due to entrapped gases such as hydrogen. On the side walls, lack of fusion porosity arises from incomplete melting or insufficient overlap between adjacent beads, leading to irregular pores. Additionally, keyhole porosity may form under excessive heat input, where vapor cavities develop within the melt pool. To reduce these porosities and improving component quality, it is essential to optimize parameters including travel speed, wire feed rate, and shielding gas composition. [13].

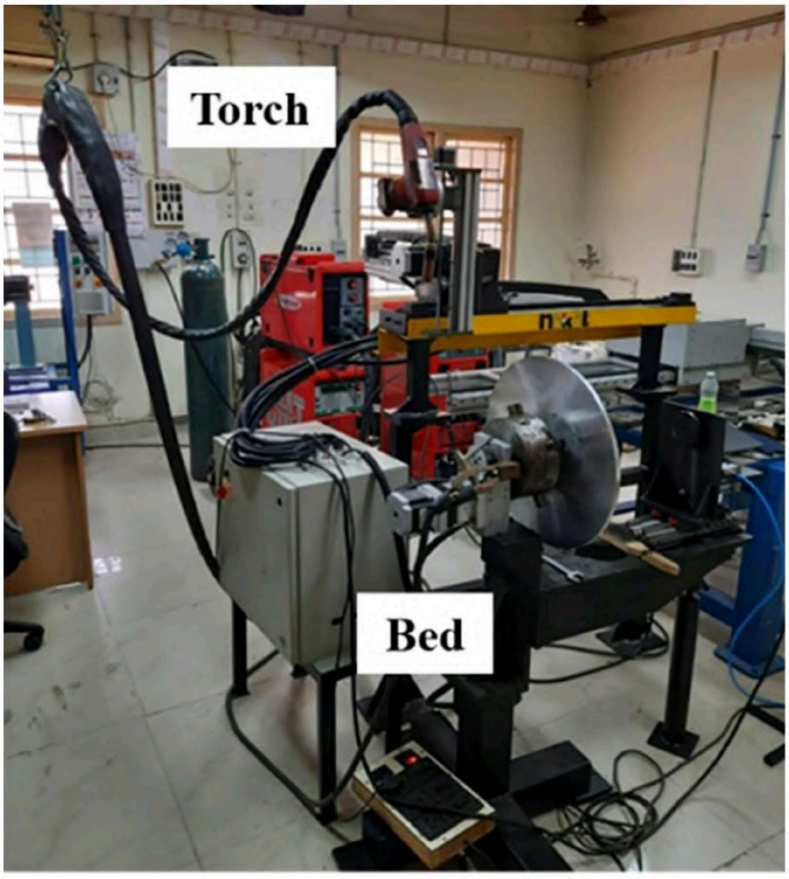

Figure 2.4: Direct Energy Deposition Setup [16]

2.7 Severe Plastic Deformation (SPD) Techniques and Their Qualities

In order to produce ultrafine grain structures and improved mechanical characteristics, severe plastic deformation (SPD) procedures apply incredibly high plastic stresses to metals without causing a noticeable change in size. Accumulative Roll Bonding (ARB), Multi-Axial Forging (MAF), High Pressure Torsion (HPT), and Equal Channel Angular Pressing (ECAP) are the SPD techniques that are most frequently used.

In ECAP, a metal billet is pressed through a die with an angled channel. imposing shear deformation without altering the billet's cross-section. It is scalable for industrial production and improves strength and ductility by grain refinement [14]. Accumulative Roll Bonding consists of stacking sheets, rolling them to bond the layers, and repeating the process multiple times, achieving significant grain refinement and enhanced mechanical behaviour [14]. Multi-Axial Forging applies repeated forging along multiple directions to accumulate strain and refine grains [14].

High Pressure Torsion (HPT), however, is distinct in its ability to impose very high shear strains under gigapascal-level compressive pressure on disk-shaped samples. It is the most effective technique for producing ultrafine or nanocrystalline grain structures, resulting in exceptional hardness and strength [15]. Among SPD methods, HPT is considered ideal for research applications on Al5356 due to its capacity for extreme grain refinement and significant reduction of internal defects.

2.8 High Pressure Torsion (HPT) post processing Effects on Al5356

HPT applies simultaneous high compressive pressure and torsional strain to small disk-shaped specimens, resulting in substantial microstructural transformation which shown in figure 2.5. During HPT processing, dynamic recrystallization occurs, fragmenting coarse grains into ultrafine or even nanometre-sized grains. This ultrafine grain structure significantly enhances the strength of Al5356 through the Hall-Petch mechanism, where dislocation motion is hindered by grain boundaries [15].

The intense deformation also increases dislocation density and grain boundary area, which substantially increases hardness, sometimes by two to three times compared to the initial state [15].

An important benefit of HPT is its ability to decrease porosity within the material. The applied high pressure compresses and closes internal pores, while the intense shear strain breaks up pore clusters and reduces microvoids. This densification improves the overall density and mechanical reliability of Al5356 parts that may have porosity inherited from casting, rolling, or additive manufacturing processes [15]. Hence, HPT is a powerful post-processing technique to enhance the performance of Al5356 components.

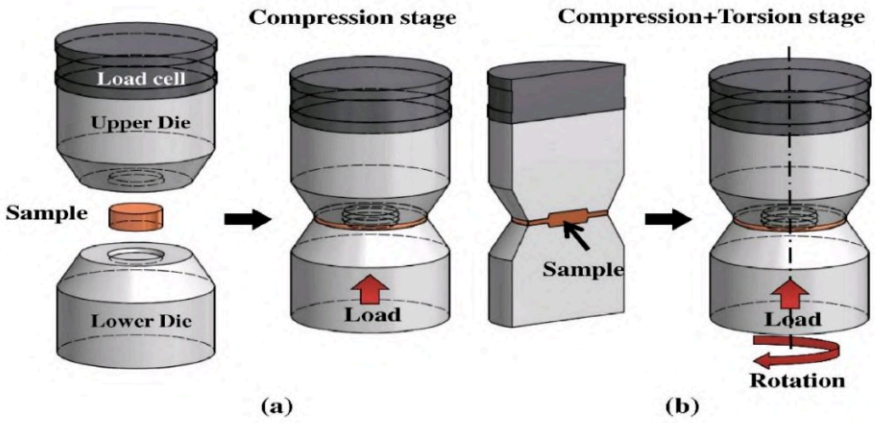

Figure: Schematic diagram of HPT process:
(a) compression stage and b) compression + torsion stage [17]

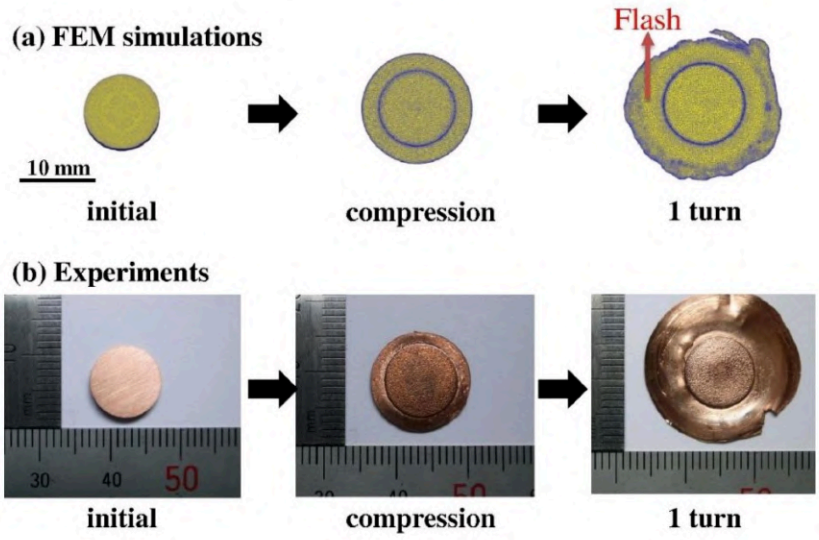

Figure 2.5: A sample's deformation: (a) simulated and (b) experimentally tested [17]

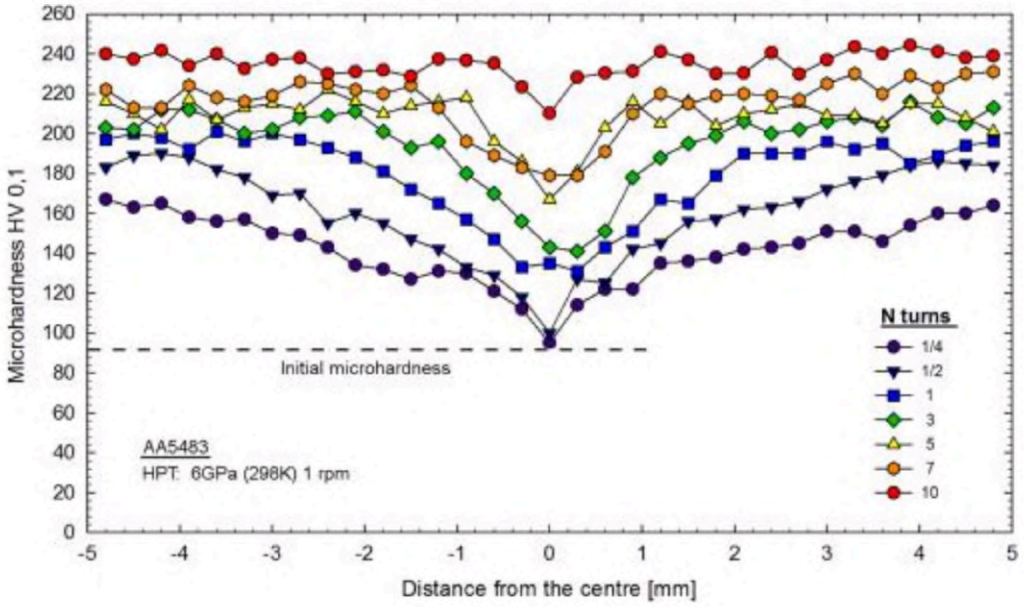

Figure 2.6. Hardness variation with distance from the disk's center for samples that underwent varying numbers of rotations during HPT processing [18].

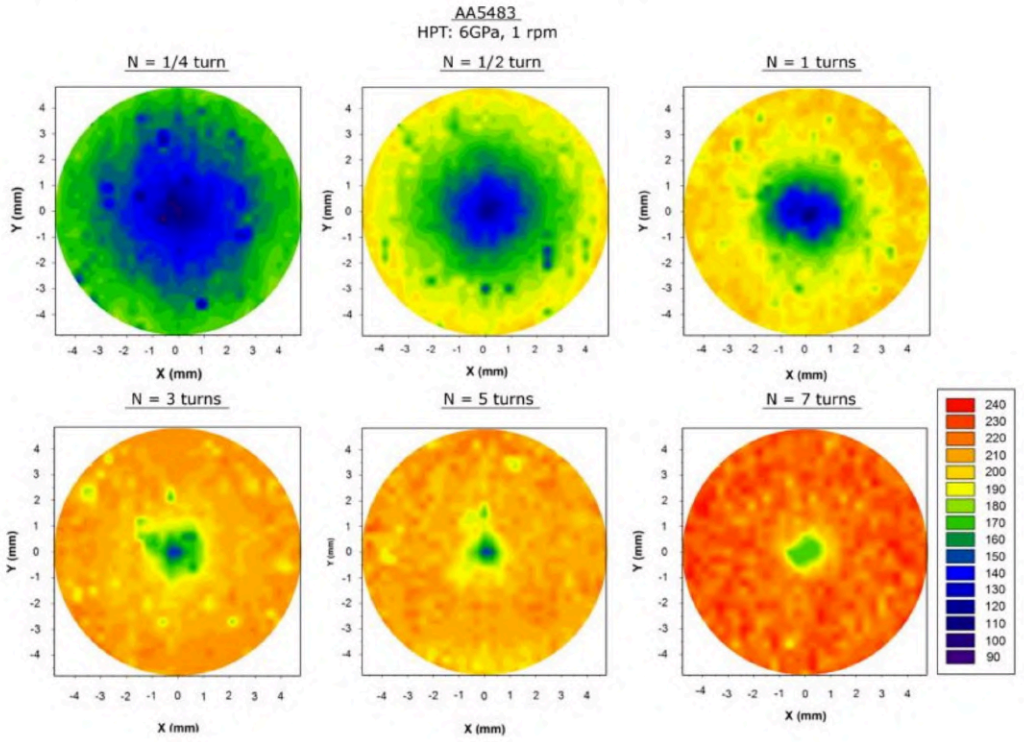

Figure 2.7: Color-coded contour maps that display the Vickers microhardness on the surfaces of disks that have undergone varying numbers of spins of HPT processing [18].

A thin disk is positioned horizontally between two gigantic anvils during HPT processing. It is then exposed to high pressure and torsional strained by one of the anvils rotating. The equivalent von Mises strain, ε, is expressed for HPT as follows to compare the shear strain with linear strain values for other SPD methods:

$$\varepsilon = \frac{2\pi rN}{\sqrt{3}h}$$

where h is the sample thickness, r is the distance from the disk's center, and N is the number of revolutions [18].

The Hall–Petch relationship, which can be used for hardness or yield flow stress, tends to be used to express how grain size influences mechanical properties. Consequently,

$$\sigma = \sigma_o + k_y d^{-\frac{1}{2}}$$

where d is the average grain size, σ_o and k_y are material constants, andσ is the flow stress at a specific plastic strain. We can write Hall Petch equation in terms of hardness as

$$H = H_o + k_H d^{-\frac{1}{2}}$$

where H_o and k_H are material constants and H is the hardness.

Table 1.2: Grain size of Al5483 [18].

Number of turns	**Grain size (nm)**		
	Center	Mid-radius	Edge
1	1050	720	580
5	600	580	550
7	310	250	240
10	280	250	250

For example, there is evidence for an inverse Hall–Petch effect at very small grain sizes from table 1.2. he Hall-Petch relationship applies to the 5483-aluminium alloy after HPT processing for 3 or more turns, and to coarse-grained samples, showing a linear correlation between microhardness and d−1/2. However, samples processed with fewer HPT turns (1/4, 1/2, and 1 turn) exhibit lower microhardness values, suggesting that a sufficient level of torsional straining is required to achieve microstructural homogeneity and consistent Hall-Petch behaviour.[18]

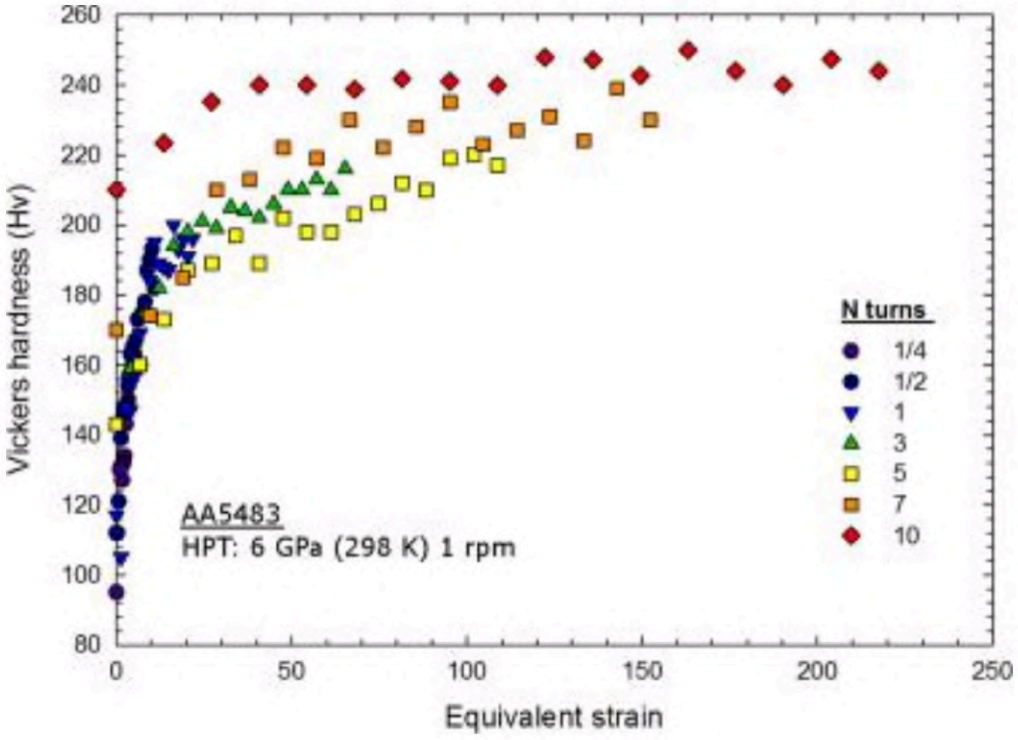

Figure 2.8: Hardness variation for samples addressed from 1/4 to 10 turns with higher equivalent strain [18].

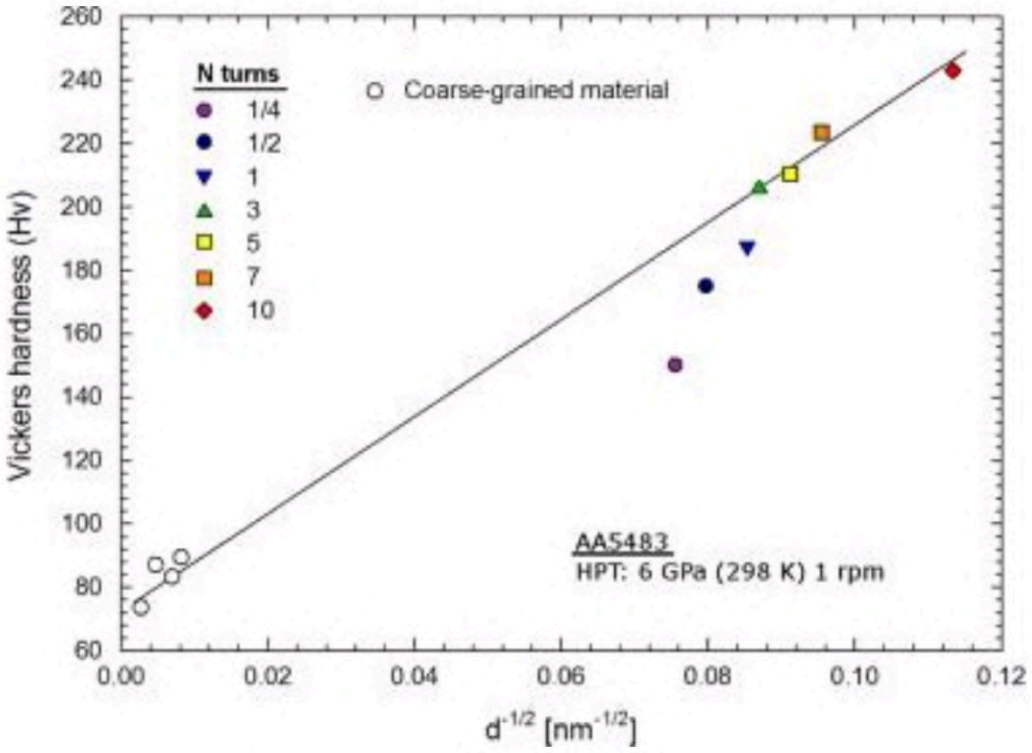

Figure 2.9: The Hall-Petch relationship for samples with coarse grains and samples that have undergone different HPT turn counts [18]

HPT processing of the AA5483 alloy, the material exhibits a significant increase in Vickers hardness with increasing equivalent strain, which is directly correlated with the number of turns, as depicted in Figure 2.5. This initial hardening is primarily attributed to extensive grain refinement, a phenomenon well-described by the Hall-Petch relationship, as validated by the linear correlation between Vickers hardness and the inverse square root of grain size in Figure 2.6. However, as the number of HPT turns increases beyond a certain threshold (approximately 7-10 turns), the Vickers hardness reaches a distinct saturation point, where further increases in strain do not yield substantial improvements in mechanical properties. This saturation signifies that the material has achieved its finest stable ultrafine-grained (UFG) or nanocrystalline (NC) structure under the given processing conditions. The observed saturation is likely due to a dynamic balance between concurrent hardening mechanisms, such as dislocation accumulation and grain refinement, and softening mechanisms, including dynamic recovery and localized dynamic recrystallization, which collectively prevent further refinement or lead to a stable steady-state microstructure. Crucially, the continued alignment of the

highest hardness values with the established Hall-Petch trend in Figure 2.6 at this saturation stage underscores that the material has reached a practical limit of grain refinement, resulting in its maximum achievable hardness without undergoing significant grain coarsening often associated with extensive static or dynamic recrystallization.

2.9 Porosity in Casting, Rolling, WAAM, and HPT: Causes and Mitigation

Porosity manifests differently depending on the manufacturing process used. In casting, porosity primarily arises from gas entrapment, particularly hydrogen, and from shrinkage during solidification. These pores reduce the load-bearing capacity of cast parts. Common mitigation techniques include degassing molten metal and controlled cooling to minimize gas solubility and solidification defects [5,6].

Rolling reduces some casting porosity by physically closing pores through compressive deformation; however, residual pores and micro-cracks often remain within rolled sheets and plates. Multiple rolling passes and subsequent heat treatments help alleviate but do not eliminate these defects [7,8].

In WAAM, porosity mainly arises due to trapped shielding gases or incomplete melting between beads, resulting in gas porosity in the melt front and lack of fusion defects on side walls. Optimizing process parameters and shielding gas flow can reduce porosity, but achieving fully dense parts remains challenging [12,13].

HPT dramatically reduces porosity by applying high pressure that compresses pores, combined with shear strain that breaks up pore clusters. This densification effect leads to near-complete elimination of porosity in severely deformed Al5356, improving density, hardness, and strength [15]. Therefore, HPT serves as an effective post-processing step to enhance parts produced by casting, rolling, or WAAM.

Table 2.3: Different processing of Al5356

Process	Porosity Type	Cause	Mitigation	Role of HPT
Casting	Gas porosity, shrinkage	Hydrogen entrapment, solidification shrinkage	Degassing, controlled cooling	HPT closes pores and densifies
Rolling	Residual pores, cracks	Incomplete closure of casting pores	Multiple rolling passes, heat treatment	HPT eliminates residual pores
WAAM	Gas porosity, lack of fusion	Shielding gas issues, insufficient melting	Optimized parameters, shielding gas	HPT densifies and refines structure
HPT	Minimal	High pressure and shear eliminate most porosity	N/A	Critical for pore closure and grain refinement

Chapter 3

Scope of study

3.1 Aim

To investigate the effect of High-Pressure Torsion (HPT) on the microstructure, physical, and mechanical properties of WAAM-fabricated Al 5356 alloy, with detailed analysis of side longitudinal and front transverse sections, and to explore its potential for improved performance in structural applications.

3.2 Objectives

This study's main goal is to analyze the mechanical, physical and microstructural characteristics of samples made using WAAM and determine whether HPT can be a used as a post-processing method to enhance those samples' qualities. This gets achieved by satisfying the following specific objectives.

- To characterize the microstructure of the as-built WAAM and HPT sample using optical microscopy and assess the presence of grain coarsening, porosity, and interlayer features.
- To determine the density and porosity of the WAAM and HPT sample using the Archimedes method.
- To evaluate the mechanical hardness of the WAAM and HPT sample using Vickers microhardness testing.
- To analyse the power law when increasing the number of turns in HPT.

Chapter 4

Experimental Work

This chapter presents the experimental procedures carried out to analyze the microstructural and mechanical behaviour of Al5356 samples fabricated by Wire Arc Additive Manufacturing (WAAM) and further processed by High-Pressure Torsion (HPT). The focus is on the preparation of samples and the methodology followed for various characterization techniques.

4.1 Sample Selection

For this study, the aluminum alloy Al5356 was selected due to its excellent corrosion resistance and mechanical properties suitable for additive manufacturing applications. The Al5356 alloy wire was chosen as the feedstock material for the Wire Arc Additive Manufacturing (WAAM) process. The chemical composition of the Al5356 alloy used is listed in Table 4.1. The alloy primarily consists of aluminum (94.513 wt%) with magnesium (4.795 wt%) as the main alloying element, along with trace amounts of iron (Fe), manganese (Mn), chromium (Cr), silicon (Si), titanium (Ti), and copper (Cu).

Table 4.1: Material Composition of Al5356

Element	**Al**	**Mg**	**Fe**	**Mn**	**Cr**	**Si**	**Ti**	**Cu**
Composition (wt%)	94.513	4.795	0.124	0.131	0.141	0.166	0.090	0.040

4.2 Sample Preparation

The aluminum alloy samples were fabricated using the Wire Arc Additive Manufacturing (WAAM) technique with Al5356 wire as the feedstock. The WAAM process parameters were carefully optimized to ensure consistent deposition and sample quality. The key parameters employed in this study are listed in Table 4.2 and include welding current, voltage, argon gas flow rate, travel speed, wire feed speed, and interlayer waiting time.

Table 4.2: WAAM Parameters for AL5356

Parameters	Value
Current	155 Amp
Voltage	15.6 Volt
Argon	14 L/min
Waiting Time	40 sec
Travel Speed	50 mm/sec
Wire Feed Speed	2.5 mm/min

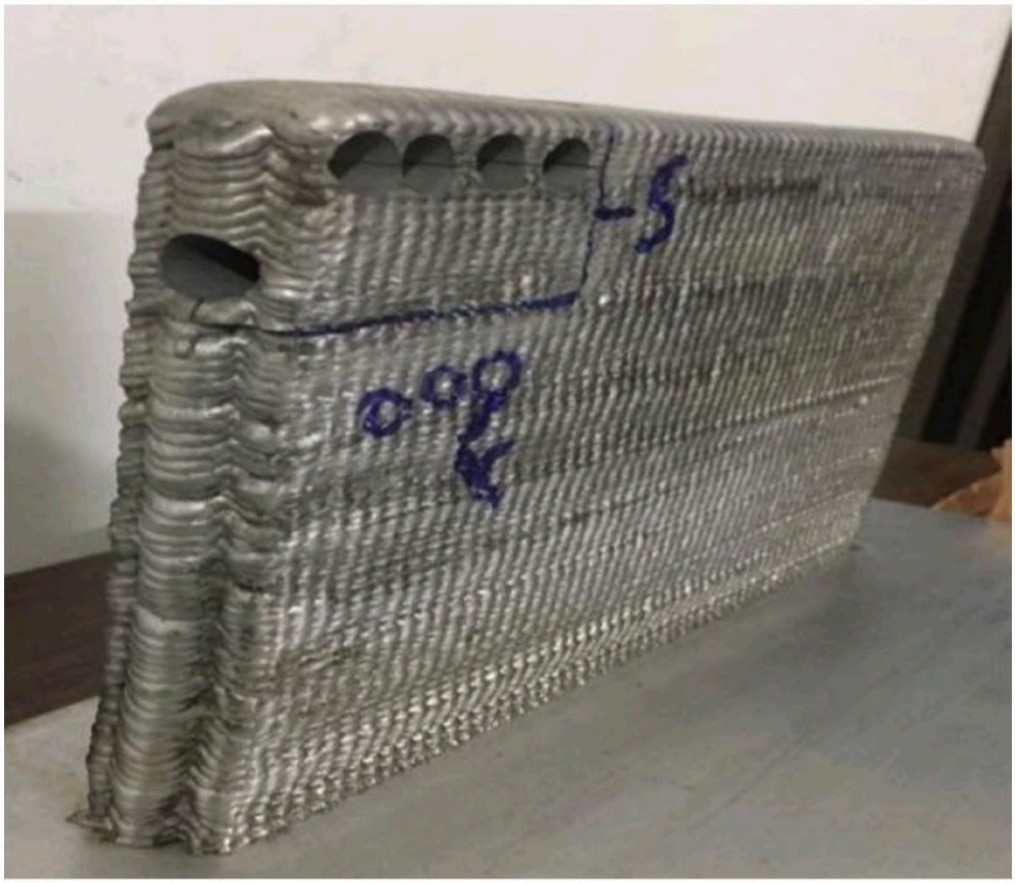

Figure 4.1: Al5356 Wall Manufactured by WAAM

After the WAAM process, a wall-like structure was fabricated layer by layer. Disk-shaped samples with a diameter of 10 mm and a thickness of 1 mm were extracted from this wall using Wire Electrical Discharge Machining (Wire

EDM), specifically from both the longitudinal direction (parallel to the build direction, taken from the side of the wall) and the transverse direction (perpendicular to the build direction, taken from the front face of the wall).

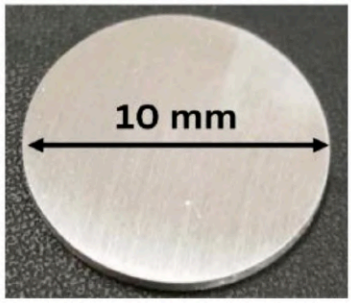

Figure 4.2: WAAM Sample Before HPT

These disks were then subjected to Severe Plastic Deformation (SPD) using the High-Pressure Torsion (HPT) technique. The HPT process was carried out under an applied pressure of 6 GPa with an angular speed of 1 rotation per minute (rpm). To investigate the influence of increasing strain on microstructure and properties, different levels of deformation were introduced by applying 0.5, 1, 5, and 10 turns during HPT processing.

Figure 4.3: WAAM Sample After HPT

4.3 Sample Polishing

All samples were initially polished for hardness testing, X-ray diffraction (XRD), and density measurements using abrasive papers starting from 80 grit to 4000 grit. For microstructural observation under an optical microscope, polishing was extended with diamond suspensions of 9 µm, 3 µm, and 1 µm. For SEM analysis, the final step involved either polishing with 0.05 µm colloidal silica or electropolishing to achieve strain-free surfaces.

4.4 Archimedes Density Test

The density of the WAAM and HPT-processed samples was measured using the Archimedes principle. A high-precision electronic balance with a density determination kit was used for the experiment. Samples were weighed in air and then in deionized water, which has a standard density of **1 g/cm³** at room temperature. The density was calculated using the formula:

$$\rho_s = \rho_{water} \frac{W_{Air}}{W_{Air} - W_{Water}}$$

where W_{Air} is the weight of the sample in air, W_{Water} is the weight in water, and ρ_{water} is the density of water (1 g/cm³).

Figure 4.4: Systematic diagram of Archimedes Density Test

4.5 Vickers Hardness Test

The Vickers microhardness test was performed to assess the mechanical strengthening effect of HPT. A load of **100 gf** was applied for **20 seconds dwell time** using a microhardness tester. Indentations were made starting from the center of the disk to the outer edge, at **0.5 mm intervals** along a diagonal path.

For each sample, measurements were taken at four different diagonal directions to ensure data accuracy and to capture possible variations in hardness across the surface. This approach allowed for the development of radial hardness profiles, helping to understand strain distribution and hardening behaviour introduced by HPT.

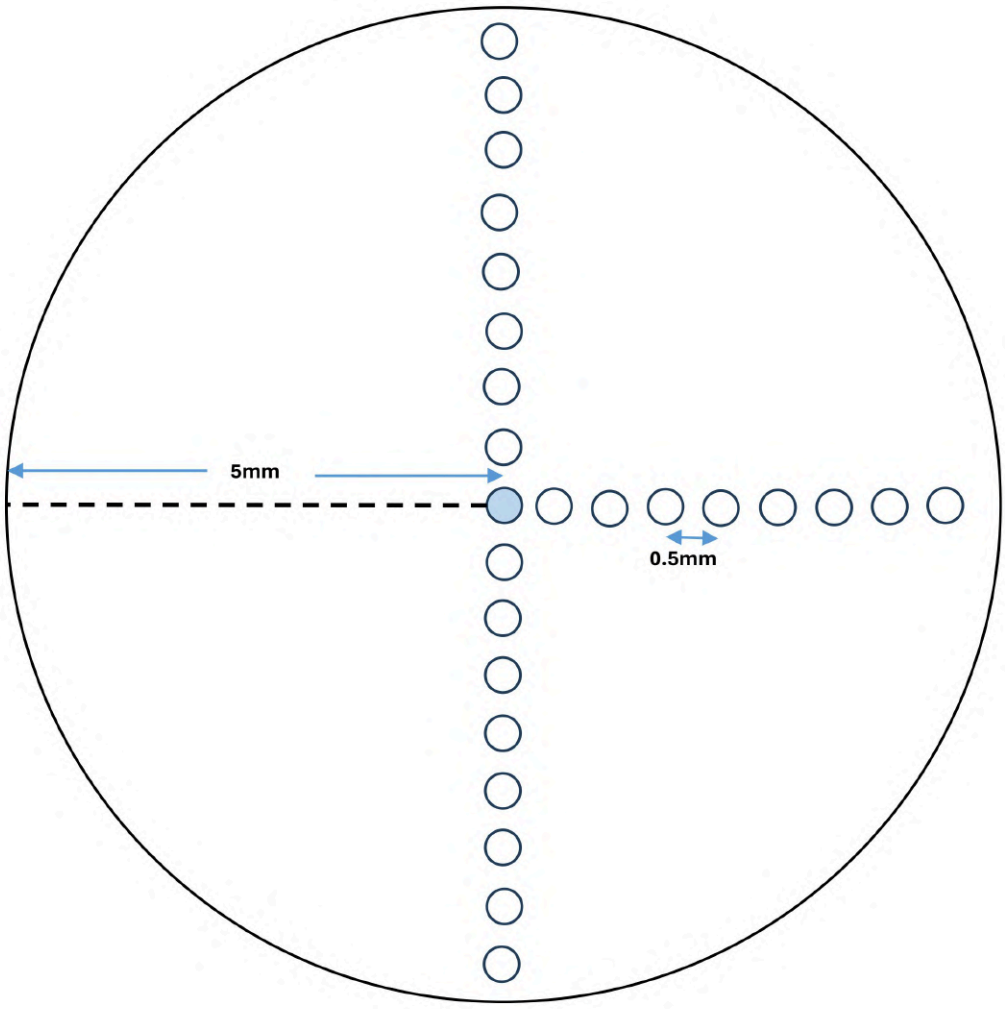

Figure 4.5: Systematic diagram for taking Microhardness

4.6 X-Ray Diffraction (XRD)

X-Ray diffraction was used to investigate the crystallographic texture and phase identification of the WAAM and HPT-processed samples. The measurements were conducted using a Cu-Kα radiation source, operated at a voltage and current suitable for aluminum alloys.

The diffraction patterns were collected at the **edge of the disk samples** for all five conditions: WAAM, HPT-0.5, HPT-1, HPT-5, and HPT-10. This location was selected to ensure analysis of the most deformed region in HPT samples, providing maximum contrast in peak broadening and texture evolution due to strain.

4.7 Optical Microscopy (OM)

Optical microscopy (OM) was used to study the microstructure of the Al5356 samples prepared by WAAM and further processed through HPT. All samples were subjected to standard metallographic preparation, concluding with a final polish using colloidal silica to achieve a mirror finish suitable for etching and microscopic observation.

To reveal fine microstructural details, **Keller's reagent** was used as the first etchant. It was prepared using 95 ml distilled water, 2.5 ml nitric acid (HNO_3), 1.5 ml hydrochloric acid (HCl), and 1 ml hydrofluoric acid (HF), and samples were etched for 10–30 seconds. This method effectively revealed grain boundaries in WAAM and HPT samples.

A **macro etchant for aluminum**, composed of 9 ml distilled water, 1 ml HCl, and 1.5 ml HF, was used for macrostructural observation, with an etching time of around 10–20 seconds. This etchant highlighted features like weld bands, interlayer interfaces in WAAM, and deformation gradients in HPT.

Finally, **electropolishing** was performed using an **A2 electrolyte** and **perchloric acid–methanol electrolyte** (ratio 2:8. This technique produced a strain-free surface, suitable for accurate microstructural characterization, especially in highly deformed zones of HPT samples.

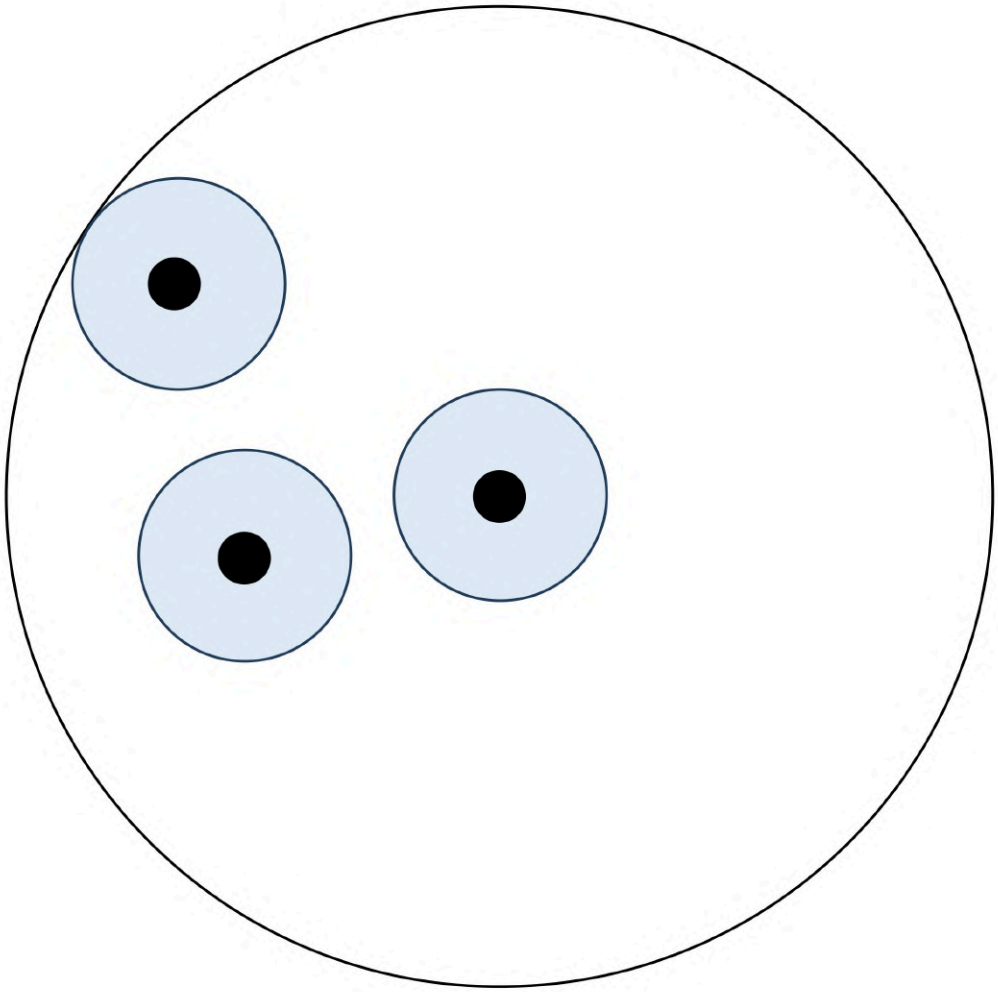

Figure 4.6: Systematic diagram for taking Microstructure

For each sample, measurements were taken at three different region to ensure data accuracy and to capture possible variations in microstructure across the surface. This approach allowed for the development of radial microstructure profiles, helping to understand strain distribution and hardening behaviour introduced by HPT.

4.8 Power Law Model

The experimentally investigate the influence of SPD on material behaviour, samples were subjected to HPT with varying numbers of turns. Following this processing, the mechanical properties were characterized using techniques such as tensile testing to obtain true stress-strain curves, from which the parameters of the power law model were determined.

$$\sigma = K(\varepsilon)^n$$

Specifically, the strength coefficient (K) and the strain hardening exponent (n) were meticulously calculated for each processed sample. Furthermore, hardness measurements, potentially employing Vickers hardness tests, were conducted to complement the tensile data, allowing for an approximate correlation between flow stress and hardness (often expressed as $\sigma \approx Hv/3$). This comprehensive experimental approach aimed to elucidate the microstructural changes and their direct impact on the macroscopic mechanical response, particularly focusing on the evolution of strength, ductility, and the validity of constitutive models under extreme deformation conditions.

Chapter 5

Results and Discussion

5.1 Density

Density is a critical indicator of material compactness and reflects the presence of voids or defects within the microstructure. The as-received WAAM samples exhibit relatively low-density values, ranging from approximately 2.56 to 2.57 g/cm³. This lower density is attributed to inherent porosity generated during the layer-by-layer additive manufacturing process, which introduces voids that reduce the overall mass per unit volume. These voids adversely affect the mechanical properties of the material by acting as stress concentrators and weak points.

Upon application of High-Pressure Torsion (HPT) processing, a marked increase in density is observed in both the Side Longitudinal (SL) and Front Transverse (FT) samples, as summarized in Table 5.1 and illustrated in Figure 5.1. Specifically, the SL sample density increases from 2.558 g/cm³ in the as-received state to 2.639 g/cm³ after 10 HPT passes. Similarly, the FT samples show a rise from 2.572 g/cm³ to 2.637 g/cm³ after just one pass of HPT.

Table 5.1: Density of Al5356 Before or After HPT on WAAM

S.No	Density (g/cm³)	Density Standard Deviation
SL As Recived	2.55796	0.00128
SL0.5	2.59851	0.0013
SL1	2.61522	0.00262
SL5	2.62815	0.00052563
SL10	2.63868	0
FT As Recived	2.57234	0.00129
FT0.5	2.59361	0.00233
FT1	2.63692	0.00237

This increase in density is primarily attributed to the severe plastic deformation and high compressive pressure applied during HPT processing. These

conditions promote significant compaction of the material, effectively closing the pores and reducing the defects originally formed in the WAAM samples. The densification achieved brings the material's density closer to its theoretical value, indicating a substantial reduction in internal voids.

Overall, these results demonstrate that HPT is a highly effective post-processing technique for enhancing the density and, consequently, the quality of WAAM-fabricated Al5356 alloys. The improved density suggests potential for better mechanical performance due to reduced porosity and defect content.

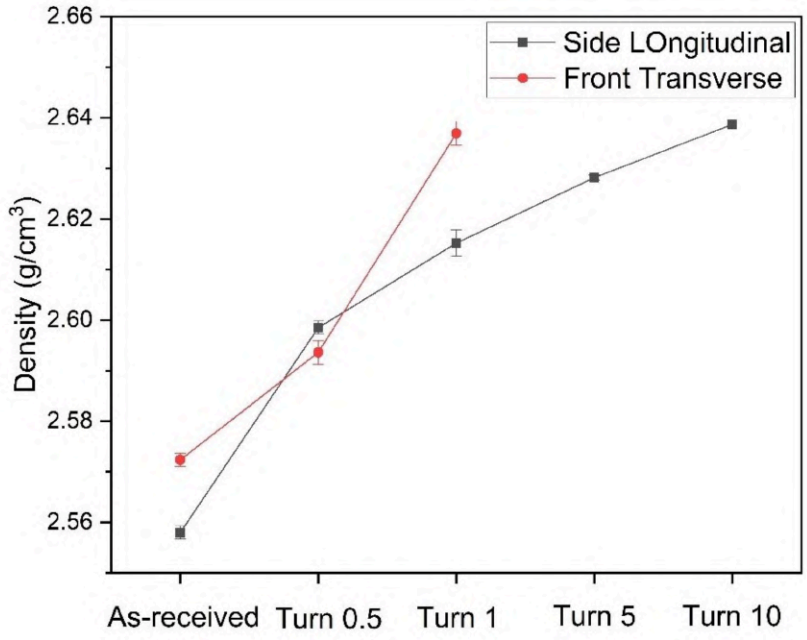

Figure 5.1: Density of Al5356 Before or After HPT on WAAM

5.2 Porosity

Porosity represents the amount of void space within a material and directly influences its strength and durability. The WAAM samples exhibit relatively high porosity levels, with Side Longitudinal (SL) samples showing approximately 3.1% and Front Transverse (FT) samples about 2.56%. These elevated porosity values are characteristic of the additive manufacturing process, where layer-by-layer deposition tends to trap gas and form voids, resulting in weak spots that can degrade mechanical performance.

Following HPT post-processing, a significant reduction in porosity is observed in both SL and FT samples, as detailed in Table 5.2 and shown in Figure 5.2. The SL samples experience a drastic decrease from 3.1% porosity in the as-received state to just 0.05% after 10 HPT passes. Similarly, FT samples show a reduction from 2.56% to 0.12% after only one HPT pass.

Table 5.2: Surface Porosity of Al5356 Before or After HPT on WAAM

S.No	Porosity (%)	Porosity Standard Deviation
SL As Recived	3.1076	0.15538
SL0.5	1.5716	0.07858
SL1	0.93882	0.09388
SL5	0.44881	0.00898
SL10	0.05	0
FT As Recived	2.56279	0.12814
FT0.5	1.75736	0.15816
FT1	0.11675	0.01051

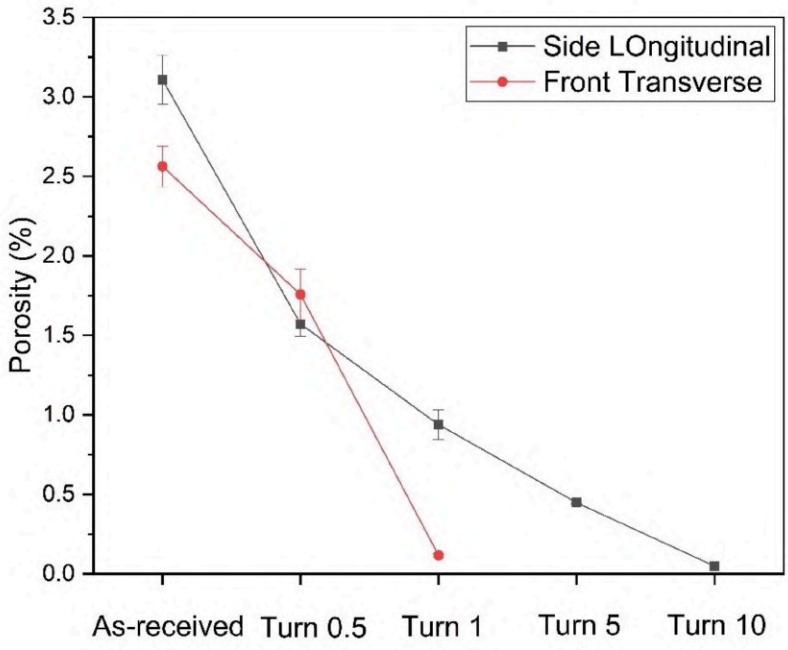

Figure 5.2: Surface Porosity of Al5356 Before or After HPT on WAAM

This substantial decline in porosity can be attributed to the intense shear forces and compressive pressure applied during HPT, which facilitate the closure of internal voids and densification of the microstructure. The ability of HPT to eliminate pores and defects is crucial for enhancing the material's mechanical integrity.

Comparing the porosity levels before and after HPT clearly highlights the advantage of HPT as an effective post-processing technique to improve the quality of WAAM-fabricated Al5356 by reducing void content and thereby enhancing its mechanical properties.

5.3 XRD

The X-ray Diffraction (XRD) analysis performed at the edge on Wire Arc Additive Manufacturing (WAAM) Al5356 samples subjected to High-Pressure Torsion (HPT) in both side longitudinal (SL) and front transverse (FT) orientations consistently revealed significant microstructural changes as a function of the number of HPT turns (N). The XRD patterns for the side longitudinal (SL) samples in Figure 5.4 and front transverse (FT) samples in Figure 5.3 both displayed prominent diffraction peaks corresponding to the (111), (200), (220), (311), and (222) planes of the face-centered cubic (FCC) aluminum lattice. In the as-received (N=0) condition, both sets of samples exhibited sharp and intense diffraction peaks, indicative of a relatively coarse-grained microstructure.

However, as the number of HPT turns increased, a consistent trend of peak broadening and reduction in intensity was observed in both SL and FT samples. For the SL samples, even at N=0.5, a slight broadening and intensity reduction suggested initial grain refinement, which became more pronounced at N=1, and then significantly broader and less intense at N=5 and N=10, pointing towards substantial grain refinement to a nanocrystalline or ultrafine-grained regime and potential saturation of grain size. Similarly, the FT samples at N=0.5 and N=1 also showed noticeable peak broadening and intensity reduction, indicating effective grain refinement comparable to the initial stages observed in the SL samples. This consistent peak broadening and intensity reduction across all HPT-processed samples, regardless of orientation, is a strong indicator of grain

refinement, as peak broadening is inversely proportional to crystallite size according to the Scherrer equation. The reduction in peak intensity can also be attributed to an increase in lattice distortions and internal strains resulting from the severe plastic deformation.

While both SL and FT samples demonstrated effective initial grain refinement, the SL samples, having been subjected to a higher number of HPT turns, allowed for the observation of grain refinement saturation, further confirming the efficacy of HPT in producing ultrafine-grained or nanocrystalline microstructures. The initial "As Received" patterns for both orientations appeared similar, suggesting comparable long-range crystalline order. No dramatic changes in relative peak intensities were immediately apparent, indicating that the HPT process did not induce strong, new crystallographic textures in the material. In conclusion, the XRD analysis conclusively demonstrates that HPT processing is an effective technique for significantly refining the microstructure of WAAM Al5356 in both side longitudinal and front transverse orientations, leading to ultrafine-grained or nanocrystalline structures at higher HPT turns, which holds promising implications for enhancing the mechanical properties of these additively manufactured alloys.

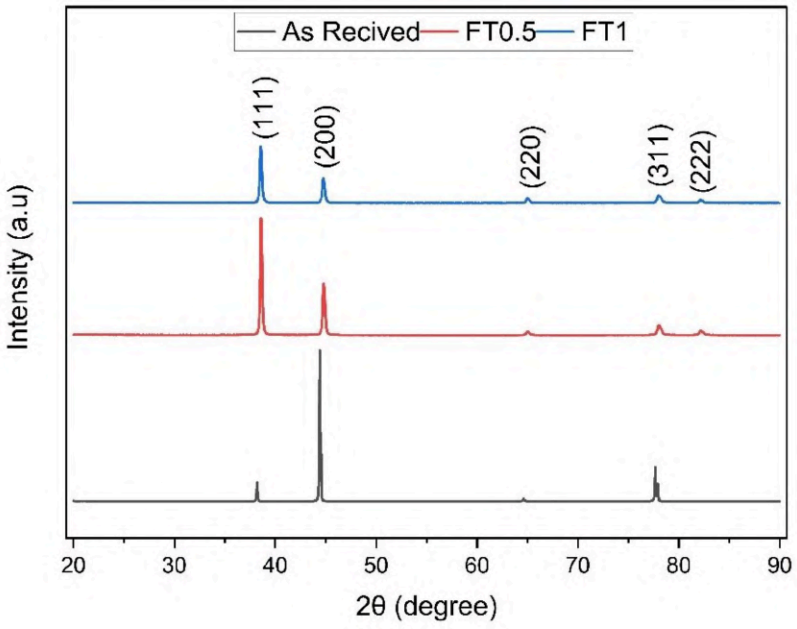

Figure 5.3: XRD of Front Transverse

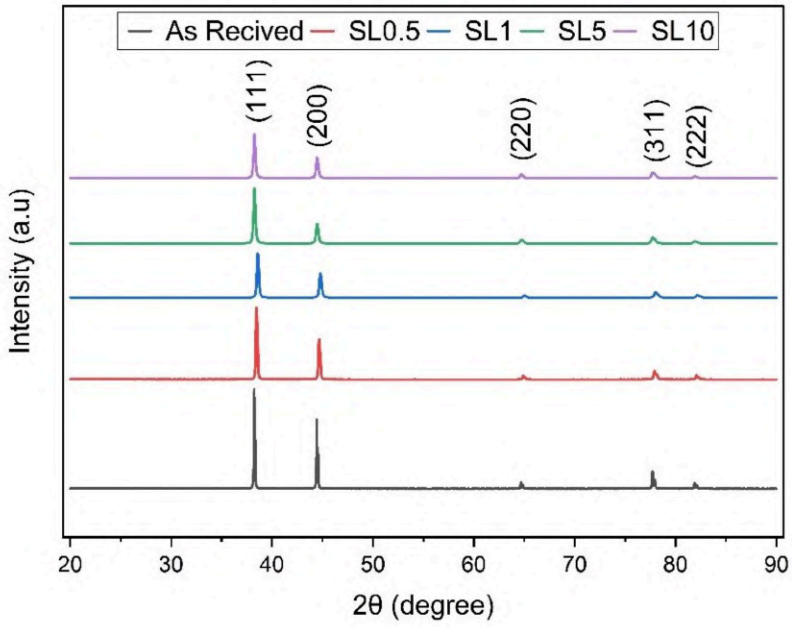

Figure 5.4: XRD of Side Longitudinal

5.4 Hardness

5.4.1 Microhardness Analysis

This section details the microhardness measurements performed on Wire Arc Additive Manufacturing (WAAM) Al5356 samples. We examined samples in their original, as-received state and after undergoing High-Pressure Torsion (HPT) processing. Hardness was measured from the center to the edge of each disk-shaped sample to understand how the HPT process affects the material's strength and its distribution.

5.4.1.1 Hardness of As-Received WAAM Al5356

As illustrated in Figures 5.5 through 5.9, the as-received WAAM Al5356 samples consistently showed a uniform microhardness. Their average hardness was approximately 70±5 HV. This consistent hardness reflects the material's microstructure as it was initially produced by the WAAM method, which typically involves a specific grain structure and some inherent manufacturing features like minor porosity. The minimal variation in hardness from the center to the edge suggests that the material was largely uniform before HPT.

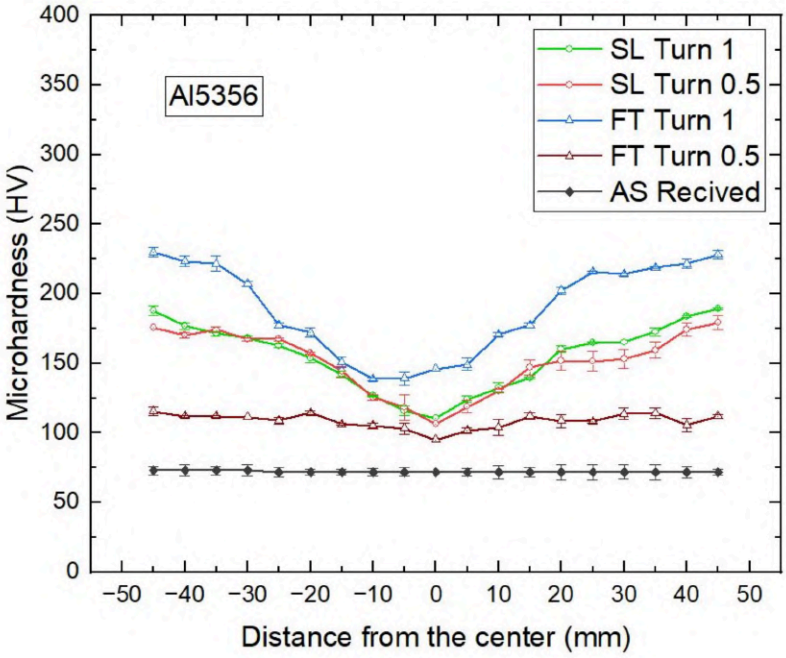

Figure 5.5: Comparison of Microhardness profiles for AS-Received, SL Turn 0.5, SL Turn 1, FT Turn 0.5, and FT Turn 1 samples across the full diameter.

5.4.1.2 Impact of HPT on Microhardness Distribution

The application of HPT dramatically changed the microhardness of the Al5356 samples. Figures 5.5, 5.6, 5.7, 5.8 and 5.9 clearly show a significant increase in hardness for all HPT-processed samples when compared to the as-received material. Additionally, a distinct "U-shaped" hardness pattern emerged, where hardness values are highest at the sample's outer edge and lowest towards its center.

For samples twisted by 0.5 turns of HPT (Figure 5.6), both "SL Turn 0.5" and "FT Turn 0.5" showed an increase in hardness. "SL Turn 0.5" samples had hardness values ranging from about 105 HV at the center to 175 HV at the edge. "FT Turn 0.5" samples followed a similar pattern, with hardness increasing from roughly 95 HV at the center to 115 HV at the edge. This initial increase confirms that HPT effectively strengthens the material even with relatively low deformation.

Increasing the HPT turns to 1 (Figure 5.7) resulted in an even greater increase in hardness and a more pronounced "U-shape" profile. "SL Turn 1" samples

showed hardness values from approximately 110 HV at the center to 185 HV at the edge. "FT Turn 1" samples exhibited an even more significant increase, ranging from about 145 HV at the center to 225 HV at the edge. This indicates that applying more deformation (more turns) leads to greater material strengthening.

From Figure 5.5 provides a comprehensive overview, comparing all HPT conditions (0.5 and 1 turns for both SL and FT) against the as-received state across the entire sample diameter. This figure clearly highlights the "U-shaped" hardness profile in all HPT-processed samples, with the lowest hardness at the center (0 mm distance) and a significant increase towards the edges (±40−50 mm). Notably, "FT Turn 1" consistently achieved the highest hardness among these conditions, followed by "SL Turn 1", "SL Turn 0.5", and "FT Turn 0.5". This suggests that both the number of turns and the specific HPT processing method (SL versus FT) influence the final hardness and how it's distributed.

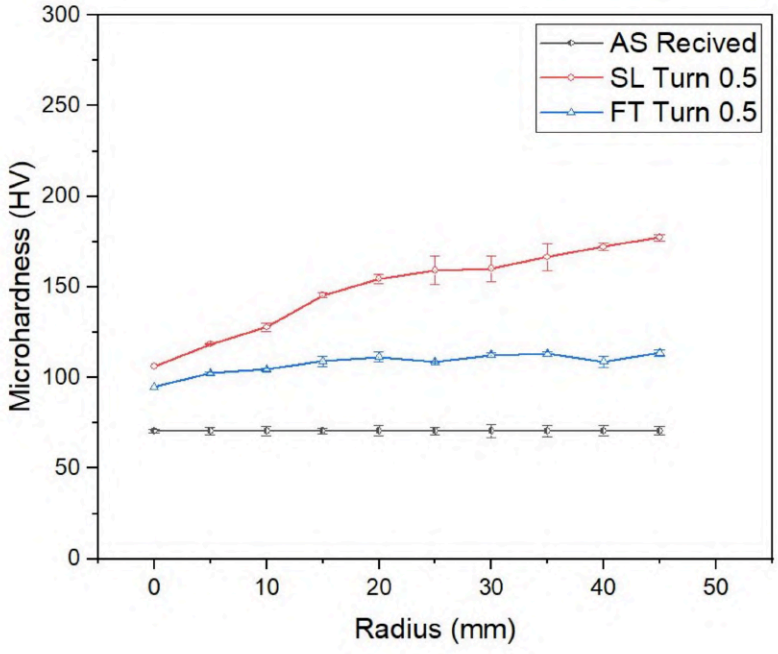

Figure 5.6: Microhardness profiles for AS-Received, SL Turn 0.5, and FT Turn 0.5 samples.

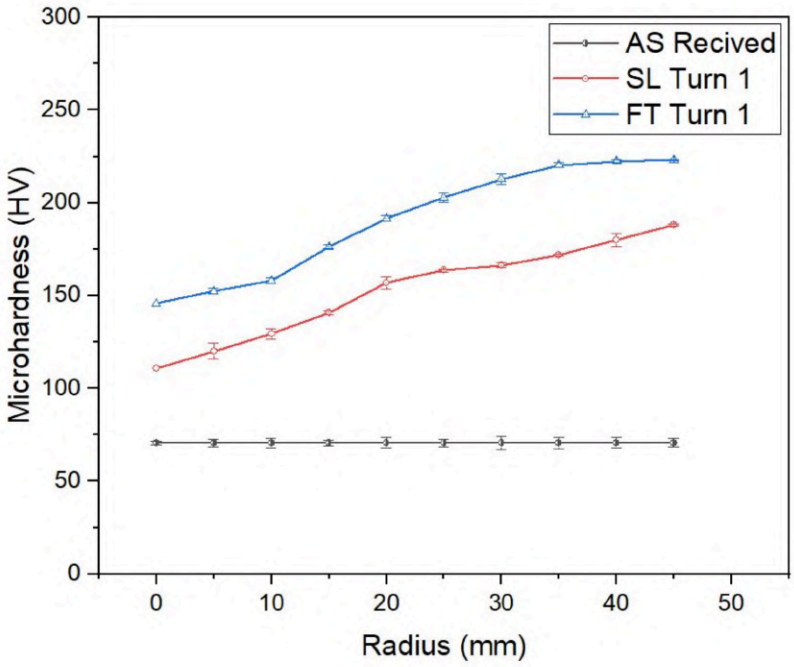

Figure 5.7: Microhardness profiles for AS-Received, SL Turn 1, and FT Turn 1 samples.

5.4.1.3 Effect of Increasing HPT Turns

From figure 5.8 specifically illustrates how increasing the number of HPT turns affects the "SL Turn" processing route (0.5, 1, 5, and 10 turns). A clear trend shows that hardness increases as the number of turns increases:

- **SL Turn 0.5:** Hardness from ≈105 HV (center) to 175 HV (edge).
- **SL Turn 1:** Hardness from ≈110 HV (center) to 185 HV (edge).
- **SL Turn 5:** Hardness from ≈150 HV (center) to 225 HV (edge).
- **SL Turn 10:** Hardness from ≈195 HV (center) to 240 HV (edge).

This continuous increase in hardness with more turns indicates that the material accumulates more plastic strain, leading to deeper changes in its internal structure. While the "U-shape" profile remains, the difference between the center and edge hardness tends to become slightly less pronounced at very high turns (e.g., SL Turn 10). This suggests that with extreme deformation, the material becomes more uniformly strengthened, even if a strain gradient still exists.

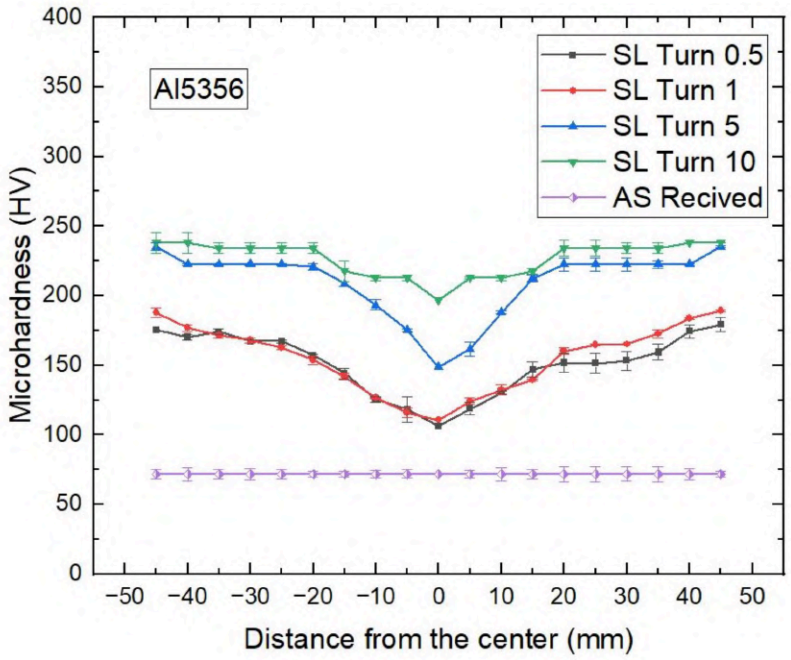

Figure 5.8: Microhardness profiles for AS-Received, SL Turn 0.5, SL Turn 1, SL Turn 5, and SL Turn 10 samples.

From figure 5.9 provides a clearer visualization of the hardness evolution at both the center and edge of the samples as the number of HPT turns increases. This figure particularly highlights the phenomenon of strain saturation. While hardness for both the center and edge increases significantly from 0.5 to 5 turns, the rate of increase noticeably slows down between 5 and 10 turns. The lines representing both center and edge hardness begin to flatten, indicating that further increases in HPT turns beyond 5 yield diminishing returns in terms of additional hardening. This visual evidence strongly supports the concept of strain saturation, where the material's microstructure has reached a stable state of refinement and dislocation density under the applied deformation.

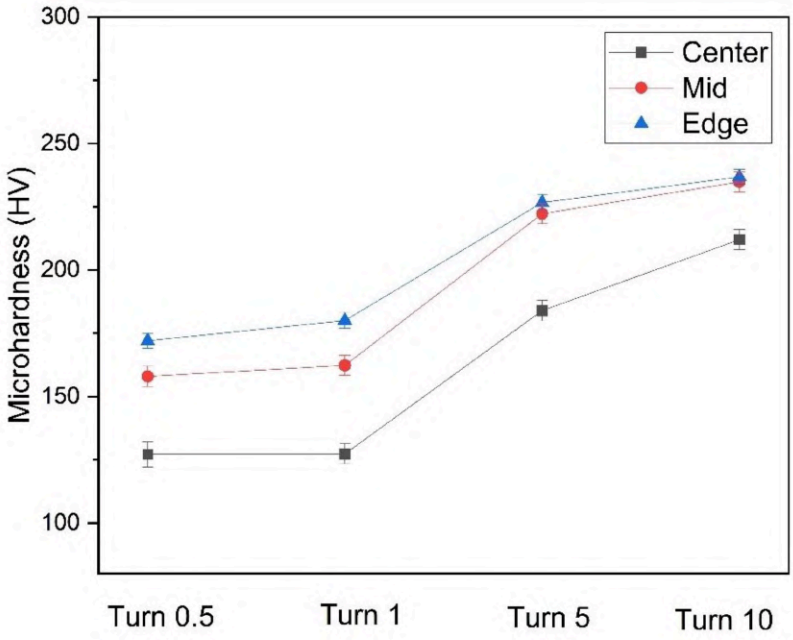

Figure 5.9: Microhardness (HV) at Center, Mid and Edge vs. HPT Turns for SL Samples.

5.4.2 Overall Hardness

The microhardness results offer valuable insights into how the internal structure of WAAM Al5356 changes when subjected to HPT. The significant increase in microhardness after HPT, compared to the original WAAM material, is primarily due to SPD, which leads to grain refinement, increased dislocation density, and work hardening. This intense twisting under high pressure causes the material's internal grains to become much smaller, forming ultrafine-grained or nanocrystalline structures, and introduces a very high number of dislocations that act as barriers to further deformation. The distinct "U-shaped" hardness profile observed in all HPT-processed samples is a direct consequence of the non-uniform strain distribution inherent to the HPT process, where the equivalent strain is zero at the center and increases linearly with radial distance, resulting in higher hardness at the periphery. A crucial part of this study involved comparing the different HPT processing conditions, particularly focusing on the initial turns (0.5 and 1) and the phenomenon of strain saturation observed at higher turns (5 and 10). While both "SL Turn" and "FT Turn" methods significantly increase hardness, "FT Turn 1" samples achieve a more substantial

increase compared to "SL Turn 1", suggesting a more efficient deformation. Furthermore, the trend for "SL Turn" samples clearly shows that hardness increases with more accumulated strain, but a notable phenomenon of strain saturation begins to appear at higher numbers of turns (especially between 5 and 10 turns), where the rate of hardness increase slows down. This indicates that the material's internal structure is approaching a stable state where further increases in deformation produce only minor additional gains in hardness, implying that the primary strengthening mechanisms are reaching their maximum potential. The observed increase in microhardness directly indicates an improvement in the overall strength of the Al5356 alloy, as SPD-processed materials typically show significantly better tensile and yield strength; however, the non-uniform hardness profile means that mechanical properties will also vary across the disk, with edges being stronger but potentially less flexible than the center, a crucial consideration for applications requiring consistent material properties.

In High-Pressure Torsion (HPT), the relationship between hardness and strain reveals a fascinating interplay of material behaviour under extreme deformation. Initially, as strain increases, the material's hardness typically rises significantly due to intense strain hardening. This is primarily driven by profound grain refinement, leading to ultrafine or nanocrystalline structures, and a dramatic increase in dislocation density, both of which impede further plastic flow. However, this hardening effect isn't limitless; beyond a certain point, the hardness tends to saturate. At these very high strains, dynamic recovery and dynamic recrystallization mechanisms begin to compete with the hardening processes, effectively balancing the rate of dislocation accumulation and grain refinement, thus preventing further substantial increases in hardness. Furthermore, due to the inherent design of HPT, the strain is non-uniform, leading to a radial gradient in hardness across the sample, though prolonged processing can often achieve a more homogeneous hardened state.

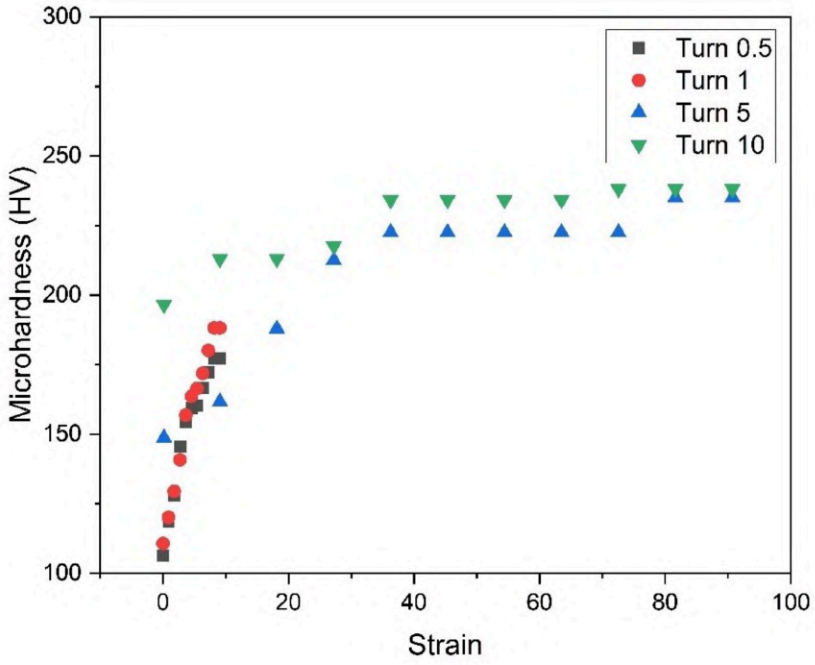

Figure 5.10:Evolution of Microhardness with Increasing Strain across the Side Longitudinal

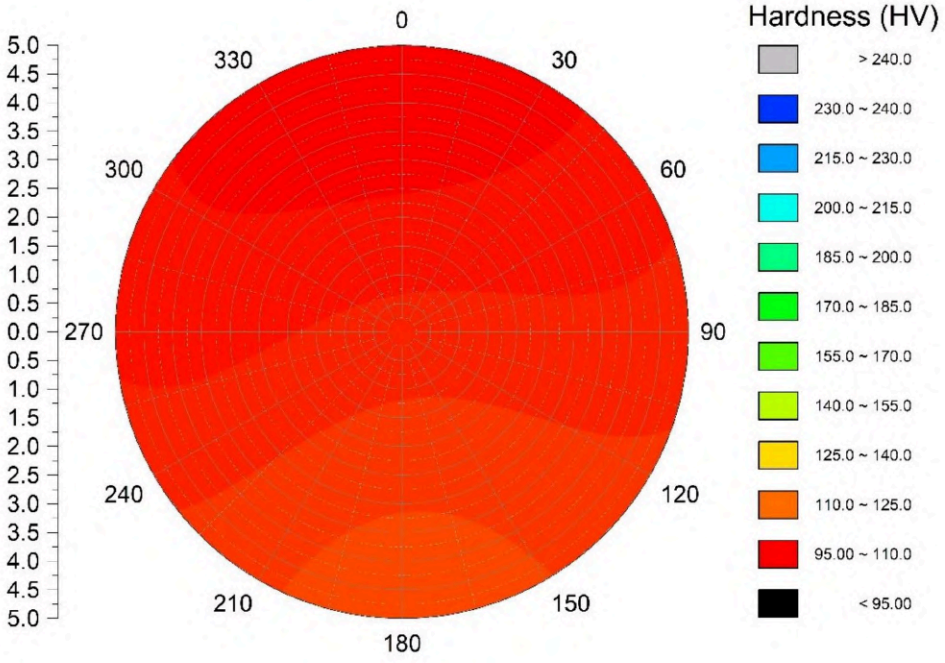

Figure 5.11:Color mapping of Front Transverse 0.5 tun

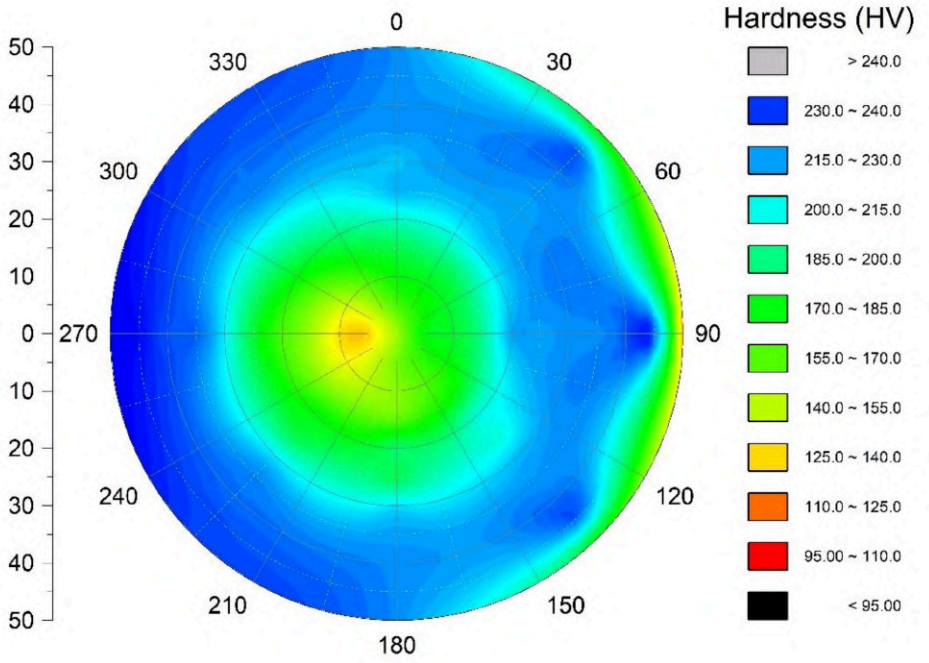

Figure 5.12:Color mapping of Front Transverse 1 tun

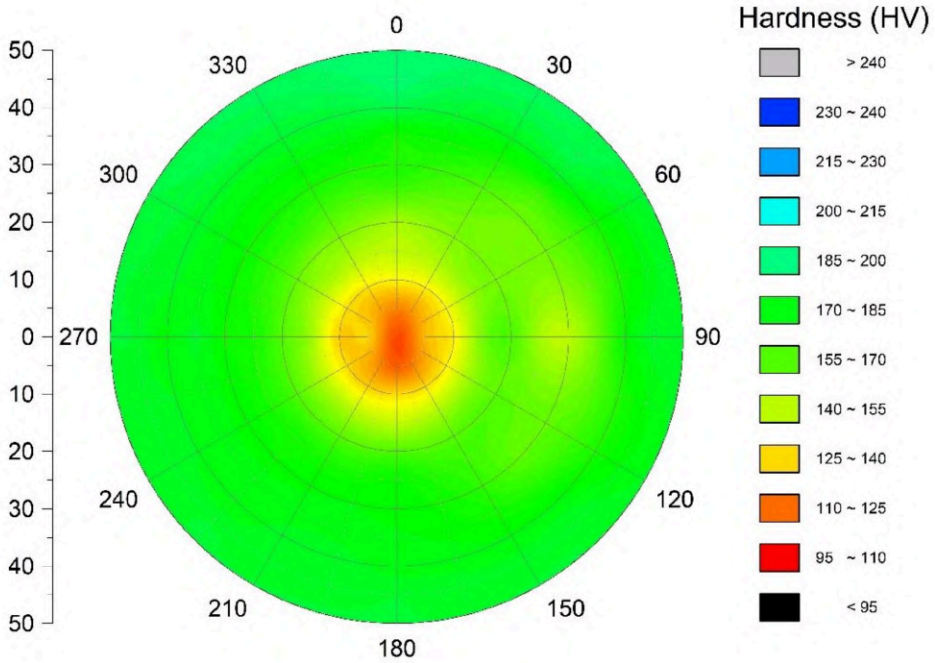

Figure 5.13:Color mapping of Side Longitudinal 0.5 tun

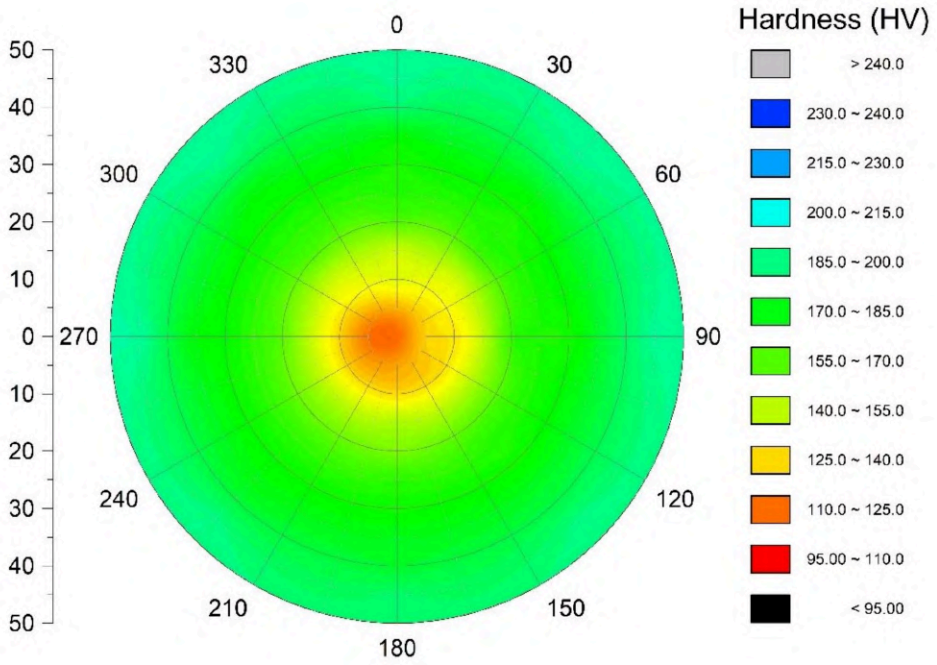

Figure 5.14:Color mapping of Side Longitudinal 1 tun

5.5 Optical Microstructure

WAAM Sample:

The use of Macro Etchant on WAAM (Wire Arc Additive Manufacturing) samples at 52 to 55 seconds resulted in successful etching, with the grain structure clearly visible. However, etching for 58 seconds led to surface burning, which destroyed the visible microstructure. This indicates that Macro Etchant is suitable for WAAM samples but requires tight control of exposure time to avoid over-etching.

In contrast, HPT (High Pressure Torsion) samples did not respond effectively to either Macro Etchant or Keller's Etchant under the tested conditions. At 40–60 seconds exposure with Macro Etchant and up to 55 seconds with Keller's Etchant, there were no observable microstructural changes. At higher exposures (80 sec with Macro Etchant and 115 sec with Keller's Etchant), burning occurred without revealing any grain structure. This indicates that the HPT

sample's microstructure is highly resistant to conventional etching, likely due to extreme grain refinement or surface compaction.

Table 5.3: Etching Trials and Observations for WAAM and HPT Samples

Sample	Etchant	Time of Exposure (sec)	Surface Appearance	Microstructural Features	Remark
WAAM	Macro Etchant	52 to 55	Visible etching	Grain structure visible	Successfully observed
WAAM	Macro Etchant	58	Surface Burn	Microstructure not visible	Failure due to burning
HPT	Macro Etchant	40	No visible effect	Microstructure not resolved	No observable changes
HPT	Macro Etchant	45	No visible effect	Microstructure not resolved	No observable changes
HPT	Macro Etchant	50	No visible effect	Microstructure not resolved	No observable changes
HPT	Macro Etchant	55	No visible effect	Microstructure not visible	No observable changes
HPT	Macro Etchant	60	Slightly effect	Microstructure not visible	No observable changes
HPT	Macro Etchant	80	Surface Burn	Microstructure not visible	Failure due to burning
HPT	Keller's Etchant	55	No visible effect	Microstructure not resolved	No observable changes
HPT	Keller's Etchant	115	Surface Burn	Microstructure not visible	Failure due to burning

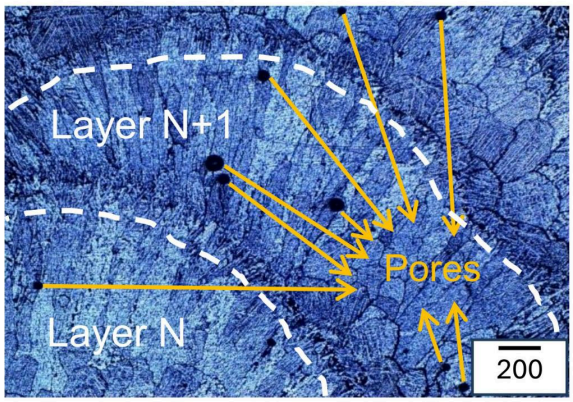

Figure 5.15: Microstructure of WAAM Al5356 (As-Built)

The microstructure of the Wire Arc Additive Manufacturing (WAAM) Al5356 sample, as depicted in Figure 5.15, clearly reveals characteristic features crucial to understanding the fabrication process and potential defects. A prominent observation is the distinct inter-layer formation, highlighted by the clear demarcation between "Layer N" and "Layer N+1". This stratified structure is inherent to the WAAM process, where successive layers of material are deposited, solidifying atop the previous one to build the desired geometry. However, intimately associated with this layer-by-layer deposition is the presence of pores, appearing as dark, somewhat spherical voids within the material. These pores are primarily generated by the trapping of inert gases, predominantly hydrogen, during the rapid solidification of the molten metal. Even with the use of argon as a shielding gas in MIG WAAM, hydrogen readily dissolves in the liquid aluminum. This hydrogen often originates from moisture on the wire surface or from ambient humidity in the welding environment that is drawn into the melt pool. As the material cools and solidifies, the dramatically reduced solubility of hydrogen in solid aluminum causes it to be rejected from the solidifying front, forming bubbles that become entrapped between the rapidly advancing solidification fronts, particularly at the interfaces of the deposited layers. Such pores constitute significant defects, acting as stress concentrators that can detrimentally impact the mechanical properties, especially the tensile strength, ductility, and fatigue life, of the WAAM-fabricated component.

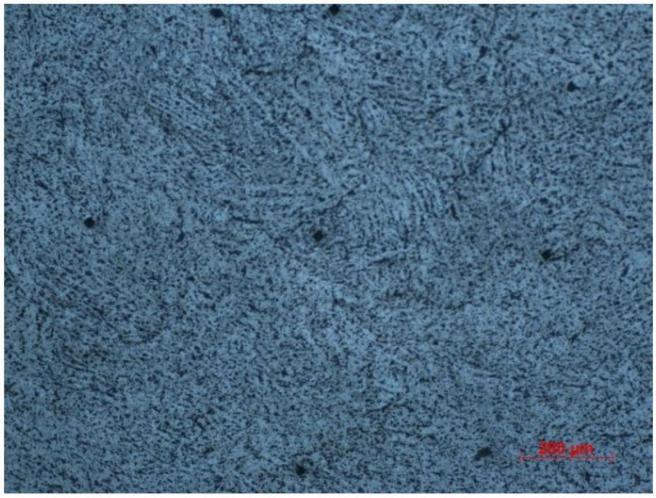

Figure 5.16: Microstructure of Front Transverse HPT (1 Turn) - Center

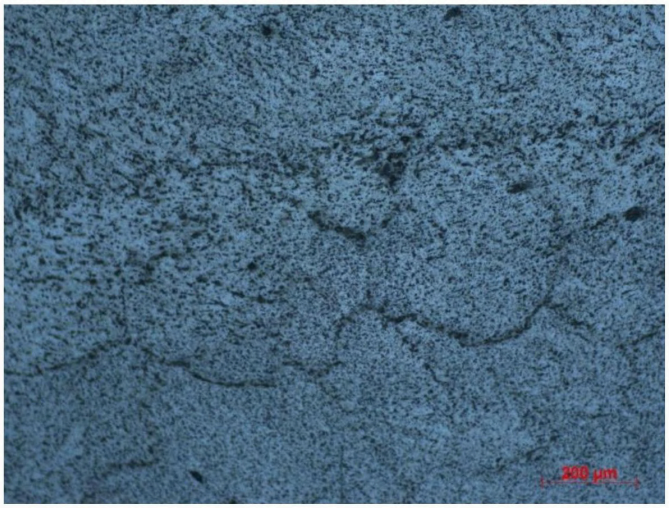

Figure 5.17: Microstructure of Front Transverse HPT (1 Turn) – Mid

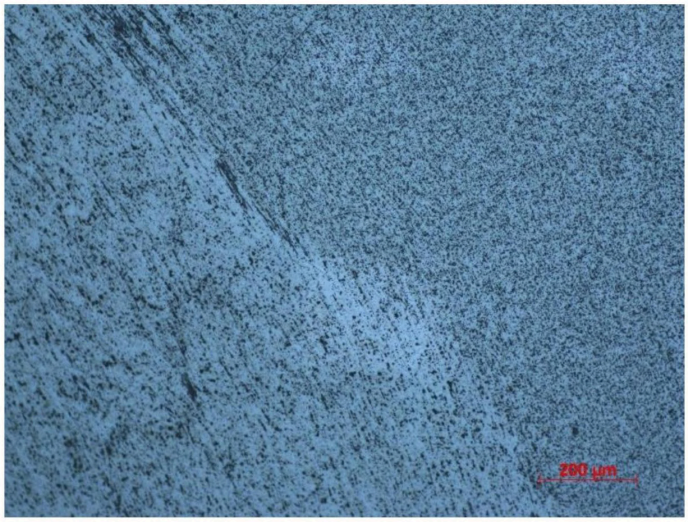

Figure 5.18: Microstructure of Front Transverse HPT (1 Turn) – Edge

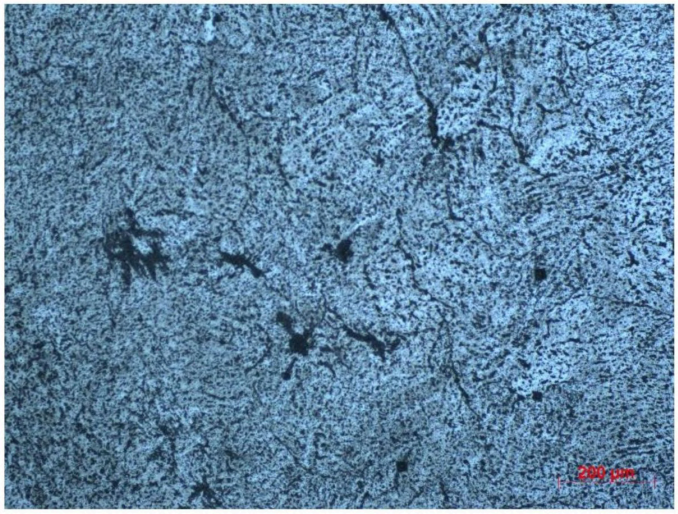

Figure 5.19: Microstructure of Side Longitudinal HPT (1 Turn) - Center

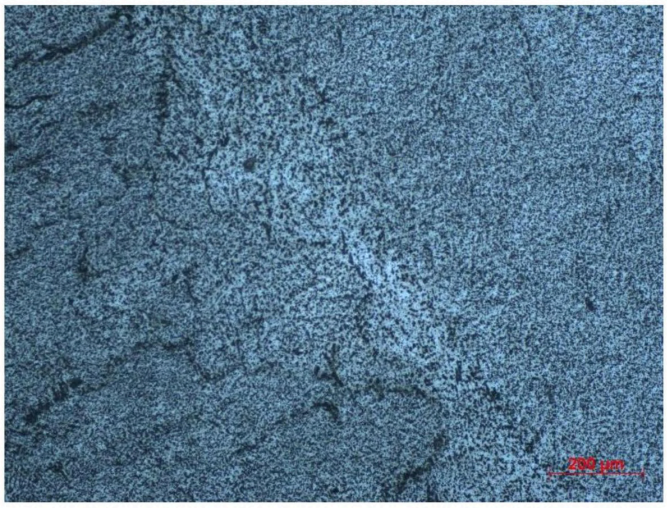

Figure 5.20: Microstructure of Side Longitudinal HPT (1 Turn) - Mid-radius

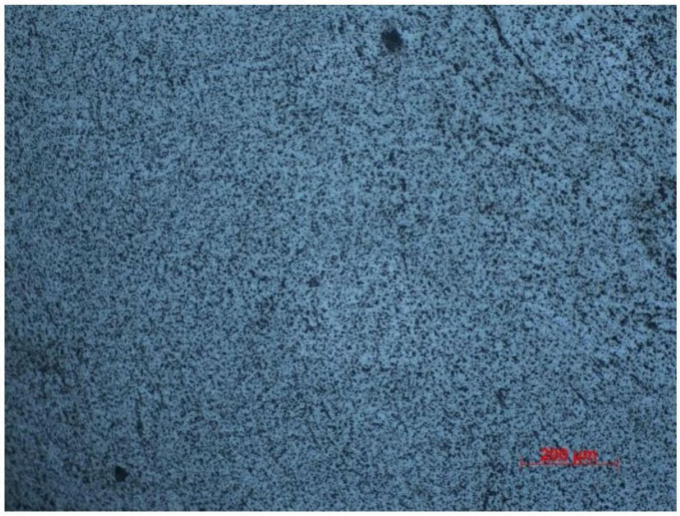

Figure 5.21: Microstructure of Side Longitudinal HPT (1 Turn) – Edge

The microstructural evolution of Al5356 subjected to Wire Arc Additive Manufacturing (WAAM) followed by High-Pressure Torsion (HPT) is critically examined through optical microscopy, with representative images presented in Figures 5.11 to 5.17. The as-built WAAM sample (Figure 5.15) clearly exhibits the characteristic layered deposition, evident from the distinct inter-layer boundaries between successive beads. Within these layers, a coarse, as-solidified dendritic or columnar grain structure is observed, typical of fusion-based additive manufacturing processes. A notable defect in the as-built state is the presence of spherical pores, particularly concentrated near these inter-layer regions. These pores are attributed to the entrapment of hydrogen gas during solidification, primarily sourced from moisture on the welding wire surface or from ambient humidity entering the weld pool, despite the use of inert argon shielding.

In stark contrast, the microstructures of the HPT-processed samples reveal a dramatic refinement of the grain structure. The front transverse (FT) sections, including Figure 5.16, Figure 5.17, and Figure 5.18, demonstrate that the original coarse features and distinct inter-layer boundaries from the WAAM process are significantly altered, indicating successful severe plastic deformation. While Figure 5.16 prominently displays indentations from hardness testing rather than intrinsic pores, the effect of HPT on defect consolidation is further elucidated by the side longitudinal (SL) sections.

The SL sections, at a higher magnification (20X), provide insights into the internal structure along the build direction and the impact on porosity. Figure 5.19, from the center of the HPT disk, shows a refined microstructure but notably contains numerous small, irregularly shaped voids, indicating that pore consolidation is less complete in regions of lower applied strain. Moving outwards, Figure 5.20, representing the mid-region, exhibits a more homogeneous and denser microstructure with a substantial reduction in the visible porosity. Finally, Figure 5.21, from the edge, presents the most refined microstructure, appearing largely dense with minimal visible porosity and clear deformation flow lines, directly confirming the extreme plastic deformation and anticipated achievement of an ultra-fine grained state. This pronounced strain gradient across the HPT-processed disk underscores its direct influence on both

microstructural refinement and the effectiveness of pore consolidation. These microstructural transformations collectively suggest a significant enhancement in the mechanical properties of the WAAM Al5356 after HPT, particularly in terms of strength, hardness, and overall material integrity, which can be correlated with the observed grain refinement and successful densification.

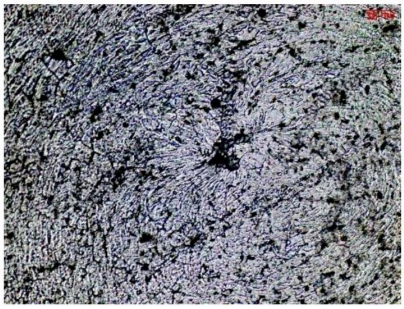

Figure 5.22: Microstructure of Side Longitudinal HPT (2 Turn) – Center

The efficacy of High-Pressure Torsion (HPT) in refining the microstructure and consolidating defects in WAAM Al5356 is further underscored by comparing samples processed with varying numbers of turns. While Figure 5.19 representing the side longitudinal section at the center after 1 HPT turn, shows significant grain refinement compared to the as-built state, it still retains numerous small, irregularly shaped voids. This indicates that at lower applied strains (characteristic of the center during 1 turn), complete pore closure is not achieved. In stark contrast, Figure 5.22, depicting the side longitudinal section from the center after 5 HPT turns, reveals a remarkably homogeneous and ultra-fine grained microstructure. The individual grains are largely unresolvable at this magnification, and the distinct irregular voids observed in the 1-turn sample are almost entirely absent, demonstrating a dramatic increase in material densification. The presence of pronounced swirling patterns in the 5-turn sample further highlights the immense plastic deformation imposed, which not only refines the grain structure to a much greater extent but also effectively consolidates porosity, even in the region of lowest shear strain within the HPT disk. This direct comparison clearly illustrates that increasing the number of HPT turns significantly enhances both microstructural homogeneity and defect elimination, leading to a more robust and improved material.

5.6 Power Law Model

The experimental investigation into the effect of increasing High-Pressure Torsion (HPT) turns on material properties, as characterized by the power law model, unequivocally demonstrated a significant enhancement in strength accompanied by a pronounced reduction in strain hardening capacity. Specifically, a substantial increase in the strength coefficient (K) was observed with higher numbers of turns, directly correlating with the severe grain refinement and increased dislocation density induced by the HPT process. This is shown in table 5.4 which is created by the analysis of figure 5.23 to 5.25.

Table 5.4: Relationship between Strength coefficient (K) and Strain hardening exponent (n)

Sample	K (MPa)	n	n at center	n at mid	n at edge
SL1	34.050	0.209	0.141	0.148	0.270
SL2	40.860	0.149	0.245	0	0.184
SL3	61.378	0.059	0.017	0	0.044

Concurrently, the strain hardening exponent (n) consistently decreased, indicating a progressive exhaustion of the material's ability to further strengthen through plastic deformation and, consequently, a diminished ductility. This is because, while HPT initially strengthens materials through microstructural refinement and increased defects, excessive deformation can lead to dislocation saturation where fewer new dislocations can be effectively generated and stored.

This saturation limits the material's capacity for uniform plastic strain, making it more prone to localized deformation and fracture at lower overall strains, effectively decreasing ductility. Furthermore, because of the significant microstructural changes and hardening mechanism saturation, the material's hardening behaviour may differ from this idealized relationship, making the basic power law model itself less valid at higher HPT turn counts. These results, which are further supported by the radial variations in the strain hardening exponent that have been observed, collectively demonstrate the trade-off that occurs in SPD, where superior strength is attained at the price of uniform

deformability and the suitability of simplified constitutive models. This information is crucial for the design and use of materials that have undergone HPT processing.

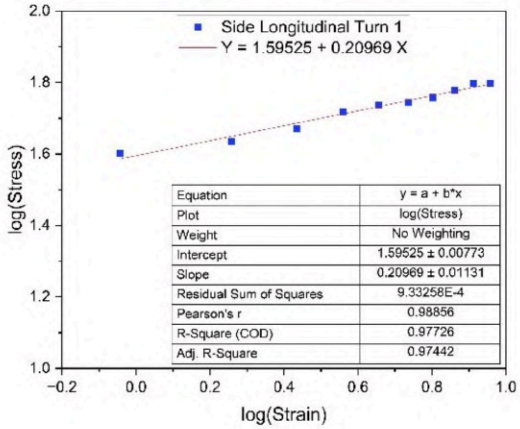

Figure 5.23: Power Law Graph of Side Longitudinal 1 Turn

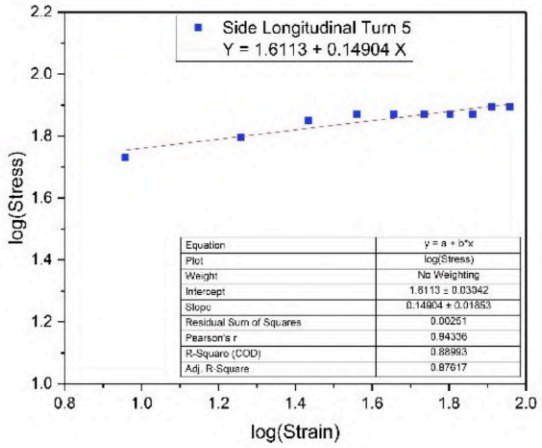

Figure 5.24: Power Law Graph of Side Longitudinal 5 Turn

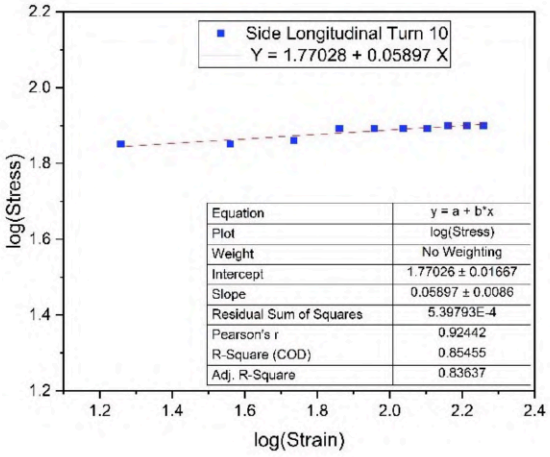

Figure 5.25: Power Law Graph of Side Longitudinal 10 Turn

Chapter 6

Conclusion and Future work

6.1 WAAM and HPT

1. Density and porosity: Density increases and surface porosity decreases with higher HPT levels. Thus, HPT from 0.5 to 10 effectively densifies WAAM material, reduces surface porosity, and improves property uniformity.
2. Microhardness increased notably with HPT. At the center, it rose from 127.17 HV (0.5 turns) to 211.95 HV (10 turns); the mid-section increased from 157.97 HV to 234.83 HV, and the edge from 172.02 HV to 236.80 HV.
3. The significant increase in microhardness confirms HPT's effectiveness in enhancing mechanical properties. Hardness rose sharply with HPT and began to plateau around 5 turns, as further increases were minimal despite continued high strain.
4. WAAM samples display coarse, equiaxed grains due to slower cooling during deposition. In contrast, SL 10-turn samples reveal finer, more uniform grains, attributed SPD from HPT.
5. The power law model becomes invalid at higher numbers of turns due to the extreme microstructural changes and saturation of hardening mechanisms induced by SPD inside the material.

6.2 Front Transverse and Side Longitudinal

1. Initially, FT WAAM is denser (2.57 g/cm^3) and less porous (2.56%) than SL WAAM (2.55 g/cm^3, 3.11%). After 1 HPT turn, FT shows better densification (2.63 g/cm^3, 0.12%) than SL (2.61 g/cm^3, 0.94%).
2. Hardness: Both SL and FT processes significantly increase hardness from the WAAM; specifically, FT1 demonstrates the most substantial hardening compared to SL0.5 and SL1 across all locations.
3. Optical Microscope: The front transverse section shows a more uniform and equiaxed grain structure due to symmetrical deformation. In contrast, the side longitudinal section reveals elongated and oriented grains along the deformation direction, indicating anisotropic flow behaviour.

6.3 Future work

1. **TEM Analysis**: Perform Transmission Electron Microscopy (TEM) on HPT-processed samples to observe ultrafine grain structures and accurately measure grain size for microstructural analysis.
2. **Mechanical Property Evaluation**: Investigate mechanical properties such as engineering stress-strain behaviour, toughness, and ductility to understand the influence of severe plastic deformation on overall material performance.
3. **Corrosion Behaviour Study**: Examine the corrosion resistance of HPT-processed samples in different environments to assess the impact of grain refinement and strain-induced defects on degradation behaviour.
4. **Texture Analysis Using EBSD**: Use Electron Backscatter Diffraction (EBSD) to examine crystallographic texture evolution with increasing HPT turns, which affects anisotropy and mechanical response.
5. **Creep and Fatigue Behaviour**: Study the long-term deformation mechanisms such as creep and fatigue to evaluate the durability of HPT-processed materials under real-world service conditions.
6. **Fractography Analysis**: Perform fractographic examination using SEM after mechanical testing to identify fracture modes and correlate failure behaviour with grain structure and deformation patterns.
7. **Comparison with Other SPD Techniques:** Compare the structural and property outcomes of HPT with other Severe Plastic Deformation techniques like Equal Channel Angular Pressing (ECAP) or Accumulative Roll Bonding (ARB) to assess processing efficiency and scalability.

References

[1] J. E. Hatch, *Aluminum: Properties and Physical Metallurgy*, ASM International, 1984.

[2] D. M. Frass and J. R. Davis, *Aluminum and Aluminum Alloys*, ASM International, 1993.

[3] G. Totten and D. MacKenzie, *Handbook of Aluminum*, Marcel Dekker, 2003.

[4] S. S. Maiti, "Mechanical and corrosion properties of Al 5356 alloy," *Materials Science and Engineering A*, vol. 527, no. 15, pp. 3676–3685, 2010.

[5] M. R. Hill and A. F. Emerson, "Porosity formation during casting of aluminum alloys," *International Journal of Metalcasting*, vol. 5, no. 4, pp. 20–27, 2011.

[6] K. P. Rao et al., "Effect of porosity on fatigue strength of cast aluminum alloys," *Materials Science and Engineering A*, vol. 528, pp. 6998–7003, 2011.

[7] A. K. Shukla and V. K. Jain, "Microstructural changes and porosity in rolled aluminum sheets," *Journal of Materials Processing Technology*, vol. 178, pp. 160–165, 2006.

[8] Y. Zhang and J. Sun, "Porosity reduction in rolled aluminum alloys," *Materials Characterization*, vol. 59, pp. 89–95, 2008.

[9] J. S. Zuback et al., "Additive manufacturing of metallic components – Process overview and state of the art," *Materials Science and Technology*, vol. 32, pp. 1016–1032, 2016.

[10] R. B. Wicker and D. H. Kruth, "Selective laser melting of aluminum alloys," *International Journal of Advanced Manufacturing Technology*, vol. 41, no. 1–2, pp. 141–150, 2009.

[11] C. G. M. Hermans et al., “Direct energy deposition of aluminum alloys: A review,” *Journal of Materials Engineering and Performance*, vol. 28, no. 5, pp. 2507–2519, 2019.

[12] S. Martina et al., “Wire arc additive manufacturing of aluminum alloys: A review,” *Additive Manufacturing*, vol. 24, pp. 232–249, 2018.

[13] L. Wang et al., “Porosity formation in WAAM aluminum alloys,” *Metallurgical and Materials Transactions A*, vol. 47, pp. 3906–3916, 2016.

[14] R. Z. Valiev and T. G. Langdon, “Principles of equal-channel angular pressing as a processing tool for grain refinement,” *Progress in Materials Science*, vol. 51, no. 7, pp. 881–981, 2006.

[15] M. Furukawa et al., “Severe plastic deformation by high pressure torsion and its effects on Al alloys,” *Materials Science Forum*, vol. 539–543, pp. 123–128, 2007.

[16] *Kumar, M. Saravana, N. Jeyaprakash, and Che-Hua Yang. "Effect of combined parametric impacts on collapsing the wall quality of WAAM Al5356 component." Engineering Failure Analysis 166 (2024): 108848.*

[17] *Lee, D. J., Yoon, E. Y., Ahn, D. H., Park, B. H., Park, H. W., Park, L. J., ... & Kim, H. S. (2014). Dislocation density-based finite element analysis of large strain deformation behavior of copper under high-pressure torsion. Acta Materialia, 76, 281-293.*

[18] *Bazarnik, P., Huang, Y., Lewandowska, M., & Langdon, T. G. (2015). Structural impact on the Hall–Petch relationship in an Al–5Mg alloy processed by high-pressure torsion. Materials Science and Engineering: A, 626, 9-15.*Kaneko, K., Hata, T., Tokunaga, T., & Horita, Z. (2009). Fabrication and characterization of supersaturated Al-Mg alloys by severe plastic deformation and their mechanical properties. *Materials transactions*, *50*(1), 76-81.

[19] Mavlyutov, A., Evstifeev, A., Volosevich, D., Gushchina, M., Voropaev, A., Zotov, O., & Klimova-Korsmik, O. (2023). The effect of severe plastic deformation on the microstructure and mechanical properties of composite from 5056 and 1580 aluminum alloys produced with wire arc additive manufacturing. *Metals*, *13*(7), 1281.

[20] Mohammadi, A., Enikeev, N. A., Murashkin, M. Y., Arita, M., & Edalati, K. (2021). Examination of inverse Hall-Petch relation in nanostructured aluminum alloys by ultra-severe plastic deformation. *Journal of Materials Science & Technology*, *91*, 78-89.

[21] Mavlyutov, A., Evstifeev, A., Volosevich, D., Gushchina, M., Voropaev, A., Zotov, O., & Klimova-Korsmik, O. (2023). The effect of severe plastic deformation on the microstructure and mechanical properties of composite from 5056 and 1580 aluminum alloys produced with wire arc additive manufacturing. *Metals*, *13*(7), 1281.

[22] Loucif, A., Figueiredo, R. B., Baudin, T., Brisset, F., Chemam, R., & Langdon, T. G. (2012). Ultrafine grains and the Hall–Petch relationship in an Al–Mg–Si alloy processed by high-pressure torsion. *Materials Science and Engineering: A*, *532*, 139-145.

[23] Wang'ombe, D. N. E. (2022). *Development of Recycled Friendly Aluminium Alloys for Automotive and Structural Applications* (Doctoral dissertation, JKUAT-COETEC).

[24] Shams, E., Abdelwahed, M., Ramadan, N., Awad, M., El-Mahallawy, N., & Taha, M. (2024). Effect of Wire Arc Additive Manufacturing Process Parameters on Bead Geometry and Porosity Formation of 5356 Aluminum alloy. *International Journal of Materials Technology and Innovation*, *4*(2), 39-45.

[25] Fu, R., Tang, S., Lu, J., Cui, Y., Li, Z., Zhang, H., ... & Liu, C. (2021). Hot-wire arc additive manufacturing of aluminum alloy with reduced porosity and high deposition rate. *Materials & Design*, *199*, 109370.

[26] Zhu, Y., Valiev, R. Z., Langdon, T. G., Tsuji, N., & Lu, K. (2010). Processing of nanostructured metals and alloys via plastic deformation. *MRS bulletin*, *35*(12), 977-981.

[27] Nakhoul, R., Montmitonnet, P., & Potier-Ferry, M. (2015). Multi-scale method for modeling thin sheet buckling under residual stresses in the context of strip rolling. *International Journal of Solids and Structures*, *66*, 62-76.

[28] Qiu, J., Murata, T., Wu, X., Kudo, M., & Sakai, E. (2013). Plastic deformation mechanism of crystalline polymer materials during the rolling process. *Journal of Materials Science*, *48*, 1920-1931.